REPUBLIC OF TURKEY

ACIBADEM MEHMET ALI AYDINLAR UNIVERSITY

INSTITUTE OF NATURAL AND APPLIED SCIENCES

INVESTIGATING THE ROLE OF HIF-1α IN REGULATING NA^+/K^+-ATPASE PUMP IN IN-VITRO ISCHEMIC HEART MODEL

GİZEM GENÇAY

MASTER'S THESIS

Department of Molecular and Translational Biomedicine

SUPERVISOR

Assoc. Prof. Emel Baloğlu

ISTANBUL – 2022

REPUBLIC OF TURKEY

ACIBADEM MEHMET ALI AYDINLAR UNIVERSITY

INSTITUTE OF NATURAL AND APPLIED SCIENCES

INVESTIGATING THE ROLE OF HIF-1α IN REGULATING NA^+/K^+-ATPASE PUMP IN IN-VITRO ISCHEMIC HEART MODEL

GİZEM GENÇAY

MASTER'S THESIS

Department of Molecular and Translational Biomedicine

SUPERVISOR

Assoc. Prof. Emel Baloğlu

ISTANBUL – 2022

Department:	Institute of Natural and Applied Sciences
Program:	Molecular and Translational Biomedicine
Thesis Title:	Investigating the Role of HIF-1α in Regulating Na^+/K^+-ATPase Pump in In-vitro Ischemic Heart Model.
Student's name and Surname:	Gizem Gençay
Date of Defense:	26/ 08/ 2022

This is to certify that I have examined this copy of master thesis. I have found that she/he prepared after fulfilling requirements specified in the associated legislations before the final examining committee whose signatures are below.

Jury president	Prof. Dr. Şevin Güney Gazi University	İmza
Supervisor of the thesis	Assoc. Prof. Dr. Emel Baloğlu Acıbadem Mehmet Ali Aydınlar University	İmza
Jury Member	Assoc. Prof. Dr. Emel Timuçin Acıbadem Mehmet Ali Aydınlar University	İmza

DECLARATION

I hereby declare that; this thesis has been written by me based on the data obtained in line with the scientific rules and ethical principles of responsible conduct of research. All information, data, comments, analyses have been collected and processed through scientific, academic writing style, and literature used have been duly shown by giving reference to the original sources in accordance with the publication ethics. I also announce and emphasize that I have not violated any rules secured by patent and copyrights whilst the conduct and writing of this research.

Gizem Gençay

Date: 26.08.2022

Signature:

ACKNOWLEDGMENT

Initially, I would like to start my acknowledgment with my supervisor Assoc. Prof. Emel Baloğlu. She always supported and motivated me in every situation. In this process, I learned a lot from her, not only about experiment or academic knowledge, but also about life. She changed my perspective on some events and allowed me to analyse events differently. Also, I learned to look and to think from a scientific perspective from her. For all of these I am grateful her. Also, I have thanks to Dr. Emre Deniz, Assist. Prof. Nazlı Keskin Toklu and Assist. Prof. Zeynep Tokcaer Keskin. They always greeted me with a smile. They always motivated and encouraged me during my undergraduate and graduate educations. I learned a lot from them.

I would like to thank my groupmate Beyza Gürler. She always tried to help and motivate me. I would like to thank to Ayşe Aydanur Kulaç, Ayşenur Çiçek, Başak Kavaklıoğlu, Gülin Baran, İrfan Baki Kılıç, Ayşegül Ekmekçi for their friendship and endless support. Acibadem University is better with you.

In this part, I would like to switch to Turkish and thank to my parents. Bana tüm hayatım boyunca destek olan, her kararımda arkamda duran, yorulup pes ettiğimde beni tekrardan ayağa kaldıran, beni yalnız bırakmayan canım annem Gülümser Gençay, babam Namık Gençay, kardeşim Buse Gençay'a çok teşekkür ederim. İyi ki varsınız, iyi ki benim ailemsiniz. Ayrıca, üzerimde çok emeği olan, daima bana güvenen ve yanımda olan teyzem Özlem Balcı Ekmekçi ve eniştem Hakan Ekmekçi'ye çok teşekkür ederim.

I am grateful to the Scientific and Technological Research Council of Turkey (TÜBİTAK) for financial supports. This project was funded by the TÜBİTAK 1001 project entitled "Identification of protein interacting partners of Na^+/K^+-ATPase pump in ischemic heart disease model" (Grant No: 119S688).

TABLE OF CONTENTS

ACKNOWLEDGMENT v

LIST OF SYMBOLS / ABBREVIATIONS ix

LIST OF FIGURES xi

LIST OF TABLES xiii

SUMMARY 1

ÖZET 2

1. AIM OF STUDY 3

2. INTRODUCTION 4

2.1. Contraction and Relaxation of the Heart 5

2.2. Na^+/K^+-ATPase (NKA) pump 7

2.3. Hypoxia 10

2.4. Hypoxia Inducible Factor (HIF) Structure 10

2.5. The HIF Pathway 12

3. MATERIALS AND METHOD 16

3.1. Materials 16

3.1.1 Buffers and Other Chemicals 16

3.2 METHOD 19

3.2.1 Cell Culture Maintenance 19

3.2.1.1 Cell Counting and Freezing 20

3.2.1.2 Cell Thawing 21

3.2.2 In-Vitro Hypoxia 21

3.2.3 HIF-1α Gene Expression Silencing Experiments 21

3.2.3.1 Whole Cell Lysate Preparation 21

3.2.3.2 SDS-PAGE and Western-Blot 22
3.2.3.3 Immunofluorescence (IF) Experiments 23
3.2.4 Cell Surface Biotinylation Experiments 24
3.2.5 Immunoprecipitation (IP) Experiments 25
3.2.6 Identification of Partners of α1 NKA by Proteomic Studies 26
3.2.6.1 Comparative Group Analysis 26
3.2.6.2 Bioinformatics Analysis 27
3.2.7 Generation of HIF-1α Knock Out H9c2 Cells by CRISPR/Cas9 System 27
3.2.7.1 sgRNA and Primer Design 27
3.2.7.2 Annealing of sgRNA Oligos 28
3.2.7.3 Golden Gate Ligation Reaction 29
3.2.7.4 Transformation 30
3.2.7.5 Colony PCR 30
3.2.7.6 Isolation of Plasmids with Alkaline Lysis Solution 32
3.2.7.7 Sanger Sequencing 32
3.2.7.8 Plasmid Preparation for Transfection 32
3.2.7.9 Midiprep Plasmid Isolation 33
3.2.7.10 Control Digestion 33
3.2.7.11 2X HBS Transfection 34
3.2.7.12. MTT Assay 35
3.2.7.13 Infection of H9c2 cells with CRISPR/Cas9 Carrying Lentivirus 35
3.2.7.14 Deleting HIF-1α from H9c2 Genome 35
3.2.8 Determination the Efficiency of Genome Modification 36
3.2.8.1 Genomic DNA isolation 36
3.2.8.2 On Target PCR optimization 36
3.2.8.3 T7E1 Assay 38

3.2.8.4 Statistical Analysis 39

4. RESULTS 41

4.1. Silencing Efficiency of HIF-1α in H9c2 Cells by Adenoviruses 41

4.2. Investigating α1 NKA Expression by Cell Surface Biotinylation Experiments . 42

4.3. Immunoprecipitation and Proteomic Studies 43

4.4 Identification of Protein interacting partners of α1 NKA by bioinformatic analysis 46

4.5 Generation of HIF-1α KO H9c2 cells 56

4.5.1 Annealing of Oligos 56

4.5.2 Colony PCR 56

4.5.3 Transfection 58

4.5.4 Optimization of PCR Conditions 59

4.5.5 Lentiviral Infection 62

4.5.6 T7E1 Assay 63

4.6 Protein Expression of HIF-1α in HIF-1α Knockout Cells with CRISPR/Cas9 Gene Editing 64

4.7 Generation of HIF-1α KO Single Cell Colonies 67

5. DISCUSSION AND CONCLUSION 69

6.REFERENCES 76

7.APPENDIX 83

APPENDIX A: Chemicals Used in This Project 83

APPENDIX B: Equipment Used in This Project 85

APPENDIX C: DNA Ladder 86

APPENDIX D: Protein Ladder 86

APPENDİX E : Plasmids that used for 3rd generation lentivirus productio 87

8. CURRICULUM VITAE 89

LIST OF SYMBOLS / ABBREVIATIONS

WHO	World Health Organization
ATP	Adenosine 5′-Triphosphate
$CaCl_2$	Calcium Chloride
cDMEM	Complete Mammalian Cell Culture Medium
cDNA	Complementary DNA
CRISPR/Cas9	Clustered Regularly Interspaced Short Palindromic Repeats/ CRISPR associated protein 9
ddH_2O	Double Distilled Water
DMEM	Dulbecco's Modified Eagle's Medium
DNA	Deoxyribonucleic Acid
dsDNA	Double Strand DNA
E. coli	Escherichia coli
EDTA	Ethylenediamine Tetra acetic Acid
ECL	Enhanced Chemiluminescence
ER	Endoplasmic Reticulum
EtBr	Ethidium Bromide
EtOH	Ethanol
FBS	Fetal Bovine Serum
FM	Freezing Medium
Fwd	Forward
gDNA	Genomic DNA
GFP	Green Fluorescent Protein

HEK293FT	Human Embryonal Kidney Cell Line
HRP	Horse Radish Peroxidase
KO	Knock-Out
LB broth	Luria-Bertani Broth
$MgCl_2$	Magnesium Chloride
MOI	Multiplicity of Infection
mRNA	Messenger RNA
MTT	3-[4,5-Dimethylthiazol-2-yl]-2,5-Diphenyltetrazolium Bromide
PBS	Phosphate-Buffered Saline
PBS-Ca-Mg	PBS containing $CaCl_2$, $MgCl_2$
PBST	Phosphate Buffered Saline Tween
PCR	Polymerase Chain Reaction
Pen-Strep	Penicillin-Streptomycin
Rev	Reverse
RNA	Ribonucleic Acid
RNase A	Ribonuclease A
RT	Room Temperature
SDS	Sodium Dodecyl Sulphate
sgRNA	Sing Guide RNA
TAE	Tris-Acetate EDTA
TBST	Tris Buffered Saline Tween
T4 PNK	T4 Polynucleotide Kinase

LIST OF FIGURES

Page

Figure 1: Na^+ transport mechanism. 6

Figure 2: Structure of NKA pump. 7

Figure 3: HIF structure and functional domains. 12

Figure 4: HIF regulation in normoxic and hypoxic conditions. 13

Figure 5: Rat HIF-1α transcript list. 27

Figure 6: Calculation formula for percent rate of modification percent according to T7E1 assay results 39

Figure 7: Efficiency of HIF-1α gene silencing in H9c2 cardiomyocytes. 41

Figure 8: Confocal image of intracellular localization of HIF-1α in normoxic and hypoxic HIF-1α silenced cells. 42

Figure 9: Effect of HIF-1α gene expression silencing on membrane and intracellular expression of the α1 NKA subunit in normoxic and hypoxic H9c2 cardiomyocytes. 43

Figure 10: IP optimization experiment 1. 44

Figure 11: IP optimization experiment 2. 45

Figure 12: Western Blot image of representative α1 NKA immunoprecipitation experiment used for proteomic studies. 46

Figure 13: α1 NKA interaction network. 50

Figure 14: α1 NKA interaction network. 50

Figure 15: Venn diagram of α1 NKA interacting proteins. 51

Figure 16: Reactome pathway analysis. 52

Figure 17: KEGG pathway analysis. 53

Figure 18: Molecular function analysis. 54

Figure 19: Cellular compartment analysis. 55

Figure 20: Gel image of annealed oligos. 56

Figure 21: Gel images of selected colonies of sgRNA at the end of colony PCR. ... 57

Figure 22: Sanger sequencing analysis of sgRNA. 57

Figure 23: Agarose gel image of the Lego G2-Puro, pMDLg-pPRE, pCMV-VSV-g and pRSV-rev plasmids cut with appropriate enzymes. 58

Figure 24: Image of transfection efficiency of HEK293FT cells. 59

Figure 25: Optimization of temperature for primers. 60

Figure 26: Optimization of temperature for HIF1α-Crispr1fwd- HIF1α-Crispr2rev with 5X Phusion GC buffer. 61

Figure 27: Optimization of temperature for HIF1α-Crispr1fwd- HIF1α-Crispr2rev with 5X Phusion HF buffer. 61

Figure 28: Dose-response curves of Puromycin treatment to check cell viability. ... 62

Figure 29: Image of H9c2 cells during Puromycin treatment after GFP expressing Lego G2 puro infection. 63

Figure 30: Agarose gel image of PCR products treated and untreated with T7 enzyme. 64

Figure 31: Protein expression of HIF-1α in knockout H9c2 cells. 65

Figure 32: HIF-1α expression in knockout cells after re-culture. 65

Figure 33: Protein expression of HIF-1α from knockout cells that were re-infected with the same amount of lentiviruses used previously. 66

Figure 34: Expression of α1 NKA subunit in membrane and cytoplasmic fraction from HIF-1α KO cells that were frozen, re-cultured and infected again. 67

Figure 35: Agarose gel image of PCR product of single cell colonies. 68

Figure 36: Summary 74

LIST OF TABLES

Page

Table 1: Examples of HIF target genes. 14

Table 2: The recipe of resolving gel (lower) for SDS-PAGE. 22

Table 3: The recipe of stacking gel (upper) for SDS-PAGE..... 23

Table 4: The list of Crispr oligos and sequences. 28

Table 5: List of annealing reaction components. 28

Table 6: Annealing reaction conditions carried out on T100™Thermal Cycler..... 28

Table 7: Golden gate ligation reaction components. 29

Table 8: Golden gate ligation reaction conditions. 29

Table 9: Colony PCR reaction components. 31

Table 10: Colony PCR conditions..... 31

Table 11: List of used enzymes and buffers..... 33

Table 12: Control digestion components. 34

Table 13: Control digestion reaction conditions. 34

Table 14: On target primers and sequences. 37

Table 15: Components of My-Taq Polymerase PCR reaction. 37

Table 16: Reaction conditions of My-Taq Polymerase PCR. 37

Table 17: Components of 5X Phusion Polymerase PCR reaction. 38

Table 18: Reaction conditions of 5X Phusion Polymerase PCR. 38

Table 19: T7 Endonuclease 1 Assay components and conditions. 39

Table 20: Specific interacting partners of α1 NKA in normoxic, hypoxic, HIF-1α silenced cells or not. 49

Table 21: Names of plasmids, suitable restriction enzymes and expected base pair lengths. 58

Table 22: Names of primers and expected sequence length values. 59

Table 23: The genetic modification rate was calculated according to the band intensity of agarose gel image..... 64

SUMMARY

In cardiomyocytes regular activity of the Na^+/K^+-ATPase (NKA) pump is essential for maintaining action potential, electrical coupling, intracellular gradients, and contractility. Necropsy materials from ischemic heart disease and cells and tissues obtained from animal models reports decreased pump activity, which has been attributed to decreased expression of the pump subunits. Decreased pump activity leads to intracellular Ca^{2+} overload, diastolic dysfunction, and arrhythmias. Hypoxia inducible transcription factors (HIF) regulate the adaptation and survival of cells in low oxygen conditions. HIF activity increases in ischemic heart diseases, hypertension, heart failure and cardiac fibrosis. The aim of this thesis is to identify the proteins that interact with the NKA pump alpha1 (α1) subunit and control the intracellular dynamics of the pump in ischemic heart disease model and the role of HIF-1α in these regulations. For this purpose, HIF-1α gene expression in H9c2 cardiomyocyte cells was silenced by shHIF-1α adenoviruses. The expression of the α1 NKA at the cell membrane and in intracellular fraction was measured by cell surface biotinylation experiments in normoxic (~19%O_2), hypoxic (1%O_2) and HIF-1α silenced cells. It was observed that membrane expression of α1 NKA decreased with hypoxia. Interacting partners of α1 NKA have been identified with proteomic and bioinformatic studies after immunoprecipitation experiments. Analyzes showed that, ER stress-related proteins such as Hsp5, Erp29, Hsp90aa1 and Hsp47 interacted with α1 NKA which increased with hypoxia and reached to normoxic level with HIF-1α silencing. Moreover, studies have been performed to generate HIF-1α knockout cell line by using CRISPR/Cas9 lentiviral system.

Keywords: Cardiac ischemia, Hypoxia, Ion transporter, Na^+/K^+-ATPase pump, Proteomic analysis

ÖZET

İn-vitro iskemik kalp hastalığı modelinde Na^+/K^+-ATPaz pompasının düzenlenmesinde HIF-1α'nın rolünün araştırılması

Kalpte Na^+/K^+-ATPaz (NKA) pompasının düzenli işlevi aksiyon potansiyeli oluşumunda, hücre içi gradientlerinin düzenlenmesinde ve kontraktilitenin devamlılığının sürdürülmesinde önemlidir. Deney hayvanlarında yapılan kardiyak iskemi modeli ve otopsi materyalleri ile yapılan çalışmalara göre NKA aktivitesi, pompanın protein ifadeleri azaldığı için inhibe olmaktadır. Pompa aktivitesindeki azalma hücre içi Ca^{2+} yüklenmesine neden olarak diyastolik disfonksiyon ve aritmiye yol açmaktadır. Hipoksi ile indüklenebilir transkripsiyon faktörleri (HIF) hücrelerin düşük oksijen düzeylerine adaptasyon süreçlerinde ve canlılıklarının sürdürülmesinde rol alır. İskemik kalp hastalıkları, hipertansiyon, kalp yetmezliği ve kardiyak fibroziste HIF aktivitesi artmaktadır. Bu tezin amacı, in-vitro iskemik kalp hastalığı modelinde NKA pompasının alfa1 (α1) alt ünitesi ile etkileşen ve pompanın hücre içi dinamiklerini kontrol eden proteinleri ve bu düzenlemelerde HIF-1α'nın rolünü araştırmaktır. Bunun için, H9c2 kardiyomiyosit hücrelerinde HIF-1α gen ifadesi shHIF-1α adenovirüsleri ile etkili bir şekilde susturuldu. α1 NKA nın hücre membran ve hücre içi ifadeleri normoksik (~19%O_2), hipoksik (1%O_2) ve HIF-1α gen ifadesi susturulmuş hücrelerde hücre yüzey biyotinlenme tekniği ile ölçüldü ve α1 NKA membran ifadesinin hipoksi ile azaldığı gözlendi. Alfa1 (α1) NKA ile etkileşen proteinler immunopresipitasyon sonrası proteomik ve biyoenformatik analizler ile belirlendi. Analizler sonucunda, Hsp5, Erp 29, Hsp90aa1 ve Hsp47 gibi ER stresi ile ilişkili proteinlerin α1 NKA ile etkileştiği, etkileşimlerin hipoksi ile arttığı ve HIF-1α gen ifadesi susturulması ile normoksik düzeylere ulaştığı gözlendi. Ayrıca, CRISPR/Cas9 lentiviral sistem kullanılarak HIF-1α geni silinmiş hücre hattı oluşturmak için çalışmalar yapıldı.

Anahtar Kelimeler: Hipoksi, İyon taşıyıcısı, Kardiyak iskemi, Na^+/K^+-ATPaz pompası, Proteomik analiz

1. AIM OF STUDY

Cardiovascular diseases are among the diseases with high incidence across the world. Most cardiovascular disease related deaths are the result of cardiac ischemia and stroke. The activity of the Na^+/K^+-ATPase (NKA) pump decreases in ischemia and heart failure. The decrease in pump function causes increased intracellular Na^+ and Ca^{2+} levels, negatively affecting cardiac function. However, it is yet unknown how NKA expression is regulated in the ischemic heart.

The activity of hypoxia-inducible transcription factors (HIFs) is essential for the cells to adapt and survive at low oxygen tension. In the ischemic heart diseases, HIF-1α activity increases. Therefore, HIF-1α may have a role in regulating the protein expression of NKA in ischemic heart. However, it is yet unknown if and how HIF-1α is involved in this process.

Therefore, the aim of this Master's thesis is to explore the regulation of α1 NKA, the catalytic subunit of the pump and the proteins that interact with it in the ischemic/hypoxic heart and also to investigate the role of HIF-1α in these interactions.

2. INTRODUCTION

According to the data of the World Health Organization (WHO), cardiovascular system diseases (CVD) are among the most common diseases that affect approximately eighteen million people all over the world and are responsible for 31% of global deaths. About 85% of CVD-related deaths are the result of cardiac ischemia and stroke (1).

Current treatment modalities against CVD vary depending on the type of underlying disease that are highly associated with wide range of symptoms (2). There are several treatment strategies such as surgery, lifestyle changes, pharmacological medications, and cardiac rehabilitation. However, due to high morbidity and mortality rates there is still a need to develop new treatment approaches (3).

Cardiac ischemia is a pathological condition associated with inadequate supply of oxygen and nutrients to the heart muscle and insufficient removal of toxic metabolites (4). Most common reason of cardiac ischemia is occlusion of the coronary arteries with thrombus due to atherosclerosis (5). Additionally, ischemia of the heart can occur in diseases such as hypertension, heart valve diseases, heart failure which increase the oxygen consumption of the heart (6,7).

While short-term ischemic attacks are usually well tolerated, prolonged ischemia can cause permanent and progressive damage to the heart tissue with the increased activities of Sympathetic and Renin-Angiotensin-Aldosterone System that negatively affect cardiac function due to structural, genomic, proteomic, metabolic changes. These changes cause remodelling of the heart, which in long term if not treated, progress into heart failure and cardiac fibrosis (8–10).

During ischemia, hypoxanthine levels increase, while glutathione, phosphocreatine and ATP levels decrease. In addition, cellular metabolic changes occur such as increased rates of glycolysis, pyruvate production, lactate accumulation and decreased intracellular pH (11). In addition, changes in intracellular ion distribution, cytoskeletal disorganisation, cell swelling, and acidosis are observed (12).

2.1. Contraction and Relaxation of the Heart

The function of the heart occurs by the contraction and relaxation mechanisms. Intracellular calcium (Ca^{2+}) is the most important ion that regulates the contraction (systole) and relaxation (diastole) of the heart.

In the healthy heart when the myocardium is electrically stimulated, voltage-dependent Na^{+} channels open, causing action potential (AP) to rise. The activity of the voltage gated Na^{+} channels increase intracellular Na^{+} levels. The action potential is transmitted to the T tubules via the sarcolemma, with the changes in the membrane potential of L-type voltage gated Ca^{2+} channels open which are densely located in the T tubules and promotes extracellular Ca^{2+} enter to the myocytes (13). Increased intracellular Ca^{2+} then binds to ryanodine receptors (RYR) on the sarcoplasmic reticulum (SR) membrane. This causes more Ca^{2+} release from the SR into the cytoplasm. Local Ca^{2+} releases generate Ca^{2+} sparks. Increased intracellular Ca^{2+} binds to the Ca-binding subunit of the thin filament protein troponin on the myofilament, and triggers contraction (14). In addition, Ca^{2+} binds to ancillary calcium binding proteins such as calmodulin and parvalbumin, which activate myosin light chain kinase (MLCK), and in turn phosphorylates the regulatory light chain of myosin (15).

Cardiac relaxation occurs by releasing of Ca^{2+} ions from troponin and other Ca binding proteins. During this phase, some of the Ca^{2+} in the cytoplasm binds to SERCA, the Ca^{2+} ATPase in the SR membrane, and is taken back into the SR for storage. Rest of the Ca^{2+} is extruded from the cell by the Na^{+}/Ca^{2+} exchanger (NCX) (16) and the ATP dependent plasma membrane calcium ATPase (PMCA) (17) (summarized in Figure 1).

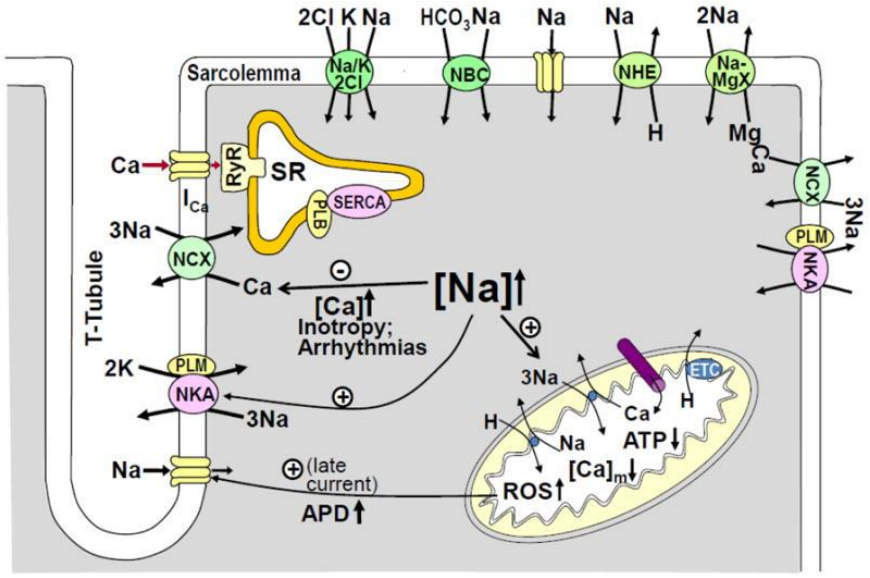

Figure 1: Na^+ transport mechanism. Basic mechanisms of regulating Na^+ transport and intracellular Na^+ in cardiomyocytes (14).

To maintain calcium homeostasis, intracellular Na^+ concentration must be kept within certain level. In myocytes, Na^+ entry into the cell is ensured by voltage gated Na^+ channels, NCX, Na^+/H^+ and Na^+/Mg^{2+} exchangers, Na^+-$HCO3^-$ and $Na^+/K^+/2Cl^-$ cotransporters (18).

The only mechanism that ensures the excretion of Na^+ out of the cell is the Na^+/K^+-ATPase (NKA) pump. All these channels, exchangers, cotransporters, and the NKA pump working in compatible maintain intracellular Na^+ in balance and indirectly intracellular Ca^{2+} levels in cardiomyocytes (19). Therefore, any changes that directly or indirectly affect the pump activity can influence the proper functioning of the heart.

2.2. Na^+/K^+-ATPase (NKA) pump

The $Na^{+/}K^+$-ATPase (NKA) enzyme or sodium potassium pump, which belongs to the P-type ATPase family, was first described by Skou in 1957 (20).

NKA is a hetero-oligomeric protein consisting of three different subunits; these subunits are catalytic α subunit, regulatory β subunit and γ subunit. The structure and organisation of NKA has been shown in Figure 2.

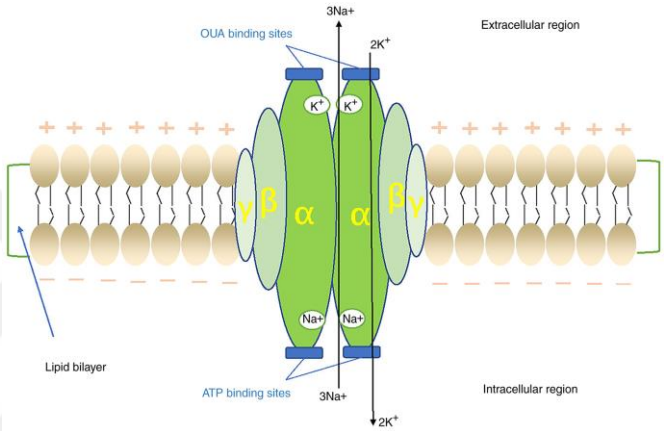

Figure 2: Structure of NKA pump. Subunit of NKA pump and ionic transports are shown (21).

Catalytic α subunit of NKA has binding sites for Na^+, K^+, Mg^{2+}, ATP and cardiac glycosides (20). There are four isoforms of the α subunit (α1, α2, α3, and α4) that are expressed differently in various tissues. The α1 NKA is expressed in all cells, α2 and α3 isoforms are expressed mostly in heart, brain, skeletal muscle. Lastly, α4 isoform has been found in the testes and adjust sperm motility (22). Moreover, localizations of each NKA isoforms are different in the cell. NKA α1 subunit is highly expressed in cell membrane while, NKA α2 and α3 subunits are mostly found in the T tubules (16,23).

Beta (β) subunit of NKA is a small, regulatory subunit and approximately 50-55 kD. Beta NKA has a significant role as a molecular chaperone and has been suggested

that it participates in insertion of the α subunit to the plasma membrane. Beta NKA consist of three different isoforms (β1, β2, β3). The β1 isoform is found in all tissues, β2 is present in heart, nervous tissue and β3 is mostly expressed in nervous tissue (21).

Third subunit is a γ subunit or FXYD family of small membrane proteins that contain seven members (FXYD1-7). FXYDs have serine residue and conserved glycine residues in the transmembrane domain. Phospholemman (PLM) is a small FXYD1 protein that is mainly expressed in heart, has significant role in the regulation of NKA. The numerous phosphorylation sites at the cytosolic carboxyl terminus of PLM make it unique. Recent research demonstrates that PLM also controls SERCA, a P-type pump closely linked to NKA (16). Unphosphorylated PLM inhibits pump activity by interacting with α and β subunits by decreasing binding affinity for internal Na^+ (24).

In the NKA structure, the α subunit has ten transmembrane (TM) domains. N terminal and C terminal regions are in cytosol. Beta subunit is near to M7-M10. While N terminal region of the β1 NKA is in the cytosol, C terminal region is in the extracellular region. In addition, γ-subunit contains one transmembrane domain near the M9 (25).

Activity of NKA in the heart muscle plays a critical role in the generation of action potential in myocytes, electrical activity, and generation of Na^+ and Ca^{2+} ion gradients and regulation of intracellular volume. Therefore, it contributes in keeping the intracellular Na^+ concentration within certain level so that the heart cells can function properly (25). NKA pumps $3Na^+$ ions out of the cell and takes $2K^+$ ions into the cell with energy obtained by hydrolysis of ATP molecule. In this way, it maintains cellular homeostasis of Na^+ and K^+ directly and indirectly affects Ca^{2+} homeostasis by modulating NCX function (26).

NCX exchanges three Na^+ ions for one Ca^{2+} ion. It is the important pathway for Ca^{2+} extrusion from cardiac myocytes. Depending on the internal and extracellular amounts of Ca^{2+} and Na^+, NCX is unusual among Na^+ transporters in that it can function in both Ca^{2+} extrusion and Ca^{2+} inflow. High intracellular Ca^{2+} activates NCX, whereas high $[Na^+]_i$ supresses NCX in a time- and $[Na^+]_i$ dependent manner. Therefore, Na^+ controls NCX activity (14).

Cardiac NKA also serve as receptor for cardiac glycosides, which enhance cardiac contractility. Cardiac glycosides bind to the α1 subunit of NKA, inhibit NKA activation and increase intracellular Ca^{2+} level by phosphorylation and activation of cSrc (27). Therefore, NKA activity and myocardial contractility are tightly related (28).

In addition, recent studies showed that NKA is not only an ion transporter, but also plays a role in intracellular signal transmission independent of this function (29,30). NKA has recently been defined as a signalling and scaffolding protein. For example, Silva et al. 2021b showed that caveolae, membrane associated scaffolding protein resident in the caveolar pool, the α1 NKA binds to cholesterol, caveolin-1 and Src. Src is a member of kinase family and NKA can turn on or off these proteins. Binding of ouabain, experimentally used cardiac glycoside, to the NKA activates Src. This induces Ras/Raf/ERK1/2 cascade and mitochondrial ROS generation (20). Cui and Xie 2017 demonstrated that several signalling proteins regulate NKA trafficking in kidney epithelial cells. For instance, dopamine promotes arrestin, GPCR kinase and 14-3-3ε recruitment to the α1 NKA, makes it easier for PI3K to attach the α1 subunit, and causes endocytosis of NKA. Another study reported that interaction of Bcl-2 proteins with NKA in fetal human lens epithelial cells (FHLCs) is essential for cell survival and death (31).

In case of cardiac ischemia, the activation of voltage-sensitive Na^+ channels increase intracellular Na^+ levels. On the other hand, ischemia decreases the activity of the NKA pump (32). The rise in Na^+ level increases the activity of other Na^+ channels and Na^+/H^+ exchangers, leading to intracellular Ca^{2+} load (33). Rising intracellular Na^+ slows down NCX, which then extrude less Ca^{2+}. This contributes more Ca^{2+} transients and contractions. However, this situation negatively affects diastolic function and causes oxidative stress and arrhythmia (34,35).

It has been suggested that the impaired activity of the NKA pump is due to decrease in protein expressions of the α1, α3, β1 subunits (36). In heart failure models using different animal species and different experimental approaches, pump activity decreased about 30%. A 40% reduction in pump activity was observed in human necropsy materials with heart failure (35,37). In the ischemic heart, the expression and

function of SERCA2 also decreases. This raises more accumulation of intracellular Ca^{2+}, contributes to reduced cardiac contractility and arrhythmia (38). It is not known exactly by which mechanisms these changes in ischemia and hypoxia occur.

2.3. Hypoxia

Molecular oxygen is the most vital element that maintains the cellular function in almost all organisms, and it is the necessary component for ATP production, required for cellular homeostasis (4). The requirement of physiological oxygen level of each cell is different. Oxygen and nutrients are delivered to all tissues via the cardiovascular system (CVS).

Hypoxia is a condition when oxygen level is not enough at the tissue for maintaining the physiological homeostasis. Hypoxia can develop in the human body under different pathological and physiological situations (39). Most CVS diseases cause reduction or cessation of oxygen and nutrition supply, and hypoxia is common in atherosclerosis, myocardial injury, pulmonary hypertension, and heart failure (40). Stroke and the growth of solid tumors are other pathogenic causes of hypoxia. Under hypoxic conditions, some physiological processes are activated such as activation of sympathetic system to compensate the changes, to increase blood flow to ischemic region, and to increase oxygen transport and delivery (41).

2.4. Hypoxia Inducible Factor (HIF) Structure

Hypoxia inducible factors (HIFs) are key proteins that are expressed in all eukaryotic species, contribute to the developmental stages, physiological functions, pathological processes of living organisms, and control the transcription of some genes to adapt cells to low oxygen levels (4).

All cells can sense hypoxia, but their response may differ from cell to cell. While some cells switch from aerobic metabolism to anaerobic metabolism to maintain their ATP production, other cells give systemic responses such as increased respiratory rate,

angiogenesis, and erythrocyte production by secreting metabolites and hormones to increase oxygen delivery to the body (41).

HIF is a heterodimer consisting of oxygen regulated an α subunit (includes HIF-1α, HIF-2α, HIF-3α) and a constitutively expressed β subunit (also called aryl hydrocarbon receptor nuclear translocator (ARNT)) (6). Each of the subunit has basic helix loop helix (bHLH) domain and Per ARNT Sim (PAS) domain that have role in heterodimerization of the subunits and allow HIF-α binding to the hypoxia response element (HRE) in the promoter of some target genes (42).

HIF-1α and HIF-2α have N terminal transactivation domain (N-TAD) and C terminal transactivation domain (C-TAD). The N-TAD domain of HIF-α is required for the activation of target genes while, the C-TAD domain interact with p300/CREB binding protein (CBP) and other transcription factors. In addition, HIF has oxygen dependent degradation domain (ODDD) that is the recognition site for the Von Hippel Lindau tumour suppressor protein (pVHL). The ODDD has two key proline residues that are hydroxylated by prolyl hydroxylase domain (PHD) enzymes (39,43). PHDs need molecular O_2, Fe^{2+} and 2-oxoglutarate as substrates for the activity. PHD enzymes hydroxylate the prolyl groups in the HIF-α structure using molecular oxygen. For hydroxylation reaction, oxygen is a crucial substrate. Therefore, PHD activity is inhibited when intracellular oxygen levels are low (44). On the other hand, β subunit has different structure that has only bHLH and PAS domain. HIF-β is ubiquitously expressed and it is not affected by intracellular oxygen level. So that, it has no transcriptional activity on its own (43).

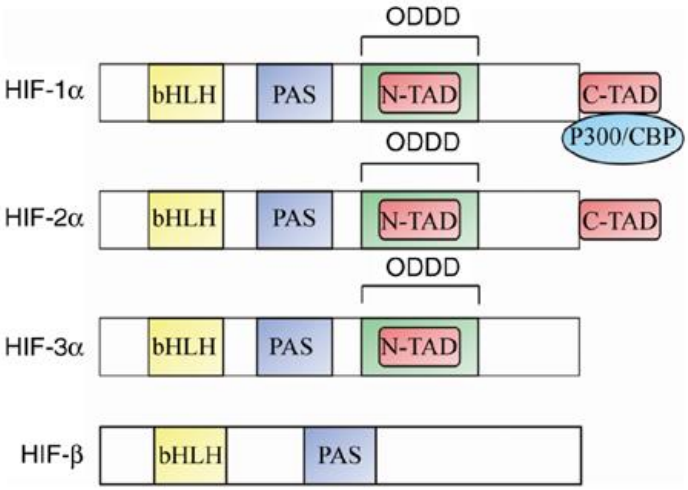

Figure 3: HIF structure and functional domains. HIF-1α and HIF-2α have a significant degree of similarity. The HIF-3α and HIF-1β have different structure from HIF-1α and HIF-2α. bHLH: basic loop helix loop, PAS: Per-AHR-ARNT-Sim, ODDD: oxygen- dependent degradation domain, N-TAD: N-terminal transactivation domain, C-TAD: C-terminal transactivation domain, PHD: prolyl hydroxylase (44).

2.5. The HIF Pathway

There are four PHD (prolyl-hydroxylase domain) enzymes that control the half-life of HIF-1α. In normoxic conditions, PHD enzymes quickly hydroxylate HIF-1α and pVHL, an E3 ubiquitin ligase, recognizes the hydroxylated subunit and tag with poly-Ub for proteasome degradation by 26S proteasome system (45,46).

In contrast, in hypoxic conditions, PHD does not hydroxylate HIF-1α due to low oxygen level. Inactivation of PHD block the binding of pVHL to the HIF-1α subunit. Consequently, HIF-1α accumulates, forms dimer with HIF-1β subunit and enters to nucleus with co-activators such as P300, CBP. Then, this complex binds to hypoxic response element (HRE) region of the target genes and activates the transcription of those genes in response to hypoxia (47) (Figure 4).

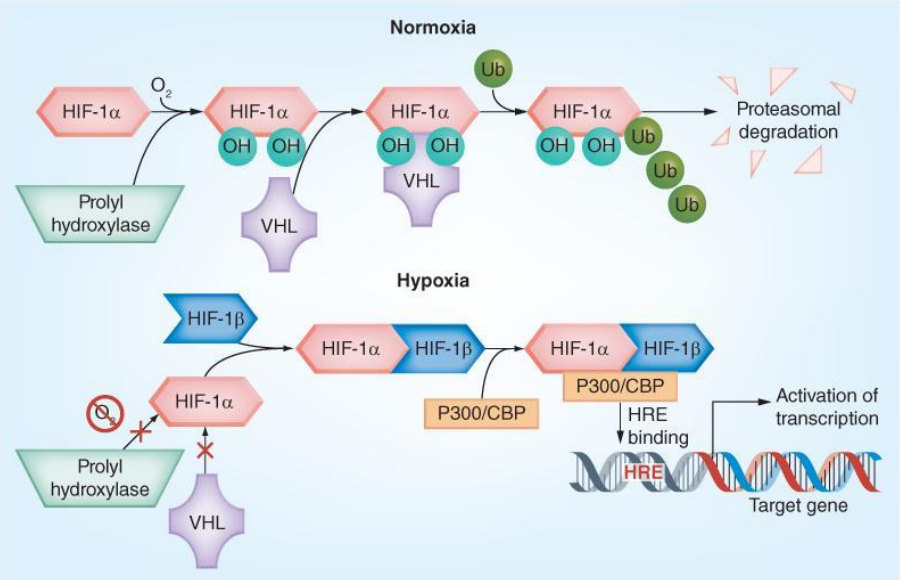

Figure 4: HIF regulation in normoxic and hypoxic conditions. In normoxic condition, PHD hydroxylates HIF-1α, which is then recognized by pVHL. This hydroxylation leads to degradation of HIF-1α in the proteasome. In hypoxic condition, since PHD is not active, HIF-1α forms dimer with HIF-1β and enters the nucleus. The dimer binds to HRE region of target gene for activation of some genes (48).

More than 1,000 human genes are regulated directly by HIF-1α. Although HIF-1α and HIF-2α increase the transcription and protein synthesis of some genes such as vascular endothelial growth factor (VEGF), placental growth factor (PGF), angiopoietin 1 (ANGPT1), ANGPT2 and platelet-derived growth factor B (PDGF-B), this effect may vary from cell to cell (6) (Table 1).

Table 1: Examples of HIF target genes. Red text demonstrates cell surface receptors while black text demonstrates secreted factors like vascular remodelling and angiogenesis (7).

Gene	Encoded protein	References demonstrating regulation by HIF-1
ADM	Adrenomedullin	82, 83
ADM2	Adrenomedullin 2 (intermedin)	84
ADORA2A	Adenosine A_{2A} receptor	83, 85
ADORA2B	Adenosine A_{2B} receptor	86
ADR1B	α_{1B}-Adrenergic receptor	87
ANGPTL4	Angiopoietin-like 4	77, 83
ANGPT1	Angiopoietin 1	14, 21
ANGPT2	Angiopoietin 2	21, 88
APLN	Apelin	89
CCL2	Macrophage chemotactic protein 1	90
CTGF	Connective tissue growth factor	91
CXCR4	CXC chemokine receptor 4	83, 92
EDN1	Endothelin 1	93, 94
EDNRB	Endothelin receptor B	95
EFNA1	Ephrin A1	96, 97
EFNB2	Ephrin B2	96
ENG	Endoglin (CD105)	98
EPHB4	Eph B4	96
EPO	Erythropoietin	17
EPOR	Erythropoietin receptor	5, 83
FLT1	VEGF receptor 1	99, 100
KITLG	KIT ligand (stem cell factor)	14, 101
LEP	Leptin	102
MDK	Midkine	103
PDGFB	Platelet-derived growth factor B	21, 75
PGF	Placental growth factor	21, 76
PROK1	Prokineticin 1	104
CXCL12	Stromal-derived factor 1	105
VEGF	Vascular endothelial growth factor	3, 106

During the embryonic development period, heart develops in a low-oxygen environment. In the early embryonic period, cardiac myocyte precursors are dependent on glycolytic pathways and oxidation of lactate as an energy source. High energy is required in the differentiation stage of adult heart cells. With the completion of the development of the mitochondria, there is a transition from glycolytic pathways to oxidative phosphorylation (49).

Adult heart cells undergo apoptosis and necrosis in an anaerobic environment, so they cannot maintain their viability for long time. The first adaptation mechanism of the heart to ischemia is to maintain the intracellular ATP homeostasis. This is achieved by transferring the energy obtained from beta oxidation of fatty acids produced in the

'adult type' of heart to glycolytic pathways and lactate oxidation. During this transition period, while the expression and activities of enzymes involved in beta oxidation decrease, those functioning in the glycolytic pathway increase (50,51). Similar changes are observed in cardiac hypertrophy and heart failure induced by pressure and volume overload (52,53). Hypertrophic heart becomes hypoxic and glycolytic metabolism is activated due to increased HIF-1α activity. In mice stably expressing HIF-1α protein and in in-vitro studies, protective effects of HIF-1α were observed in short-term cardiac ischemia by regulating angiogenesis, vascular remodelling, glucose, and redox homeostasis. However, long time stabilization of HIF-1α caused cardiac decompensation (4).

HIFs may be involved in regulating NKA in the ischemic/hypoxic heart. This thesis focused on this hypothesis by investigating the role of HIF-1α in regulating the expression of α1 NKA and interacting protein partners in in-vitro hypoxic cardiomyocytes as a commonly used model to mimic ischemic heart.

3. MATERIALS AND METHODS

3.1. Materials

3.1.1 Buffers and Other Chemicals

LB broth: 25 g LB broth was dissolved in 1L ddH_2O. The solution was autoclaved for 15 min at 121ºC and kept at room temperature (RT).

LB (Luria Bertani) broth/agar: 25 g LB broth and 15 g agar were mixed and dissolved in 1L ddH_2O. The mixture was autoclaved for 15 min at 121ºC. When the solution was cooled, it was mixed with 1 ml 100 mg/ml ampicillin, and poured into plates, kept at +4ºC.

Ampicillin (100mg/mL): 1 g ampicillin was dissolved in 10 ml ddH_2O and was filtered through 0.44 µm filter, kept at -20ºC.

Bacterial Glycerol Stock: 115 µl of 87% glycerol and 885 µl of bacterial suspension were mixed, kept at -80ºC.

EDTA (Ethylene Diamine Tetra acetic Acid) (0.5M): 18.612 g EDTA dihydrate powder was dissolved in ddH_2O, pH was adjusted to 8.00 by NaOH pellets and kept at RT.

50X TAE Buffer: 242 g Tris Base, 100 ml of 0.5M EDTA and 57.1 ml glacial acetic acid were mixed, and final volume was completed with ddH_2O to 1L.

Alkaline Lysis Solution I (AI): 50mM glucose, 25mM Tris-Cl (pH 8.00), and 10mM EDTA (pH 8.00) were mixed, autoclaved for 15 min at 121ºC and kept at +4ºC.

Alkaline Lysis Solution II (AII): 400 µl 5N NaOH and 1000 µl 10% (w/v) SDS and 8,6 ml ddH_2O were mixed. The solution was freshly prepared just before the experiment and stored at RT for short term.

Alkaline Lysis Solution III (AIII): 60 ml potassium acetate (5M) and 11.5 ml glacial acetic acid were mixed; volume was adjusted to 100 ml with ddH_2O and stored at +4ºC.

Tail Lysis Buffer: 5 ml 1M Tris (pH 8.00), 10 ml 5M NaCl, 10 ml 0.5M EDTA (pH 8.00), 25 ml 10% SDS were mixed in final volume 500 ml and stored at RT.

2X HBS (Hepes Buffer Saline): 0.8 g of NaCl (140mM), 0.027 g of $Na_2HPO_42H_2O$ (1.5mM), 1.2 g of HEPES (50mM) were mixed and volume was completed to 100 ml with ddH_2O. pH of buffer was adjusted to 7.00 by NaOH pellets and buffer was filtered with 0.22 µm filter, kept at -20°C.

Gelatine (0.1%): 0.25 g gelatine was dissolved in 250 ml ddH_2O and autoclaved for 15 min at 121ºC, kept at +4 ºC.

Mammalian Cell Freezing Medium (FM): 5 ml DMSO and 45 ml medium containing 10% FBS were mixed, medium was filtered and stored at -20°C.

10X Running Buffer: 30 g Tris base and 144 g glycine were dissolved in ddH_2O in 1L final volume. pH was fixed to 8.3 by HCl and kept at +4°C.

10X Wet Transfer Buffer: 40 g Tris Base and 144 g glycine were dissolved in ddH_2O at 1L final volume. pH was adjusted to 8.3 by HCl and kept at RT.

10X TBS: 24.2 g Tris base and 80 g NaCl were mixed in ddH_2O at 1L final volume, pH was adjusted to 7.6 by HCl and kept at RT.

10X PBS without Ca/Mg: 80 g of 1.37 M NaCl, 2 g of 24 mM KCl, 7.7 g of 43 mM Na_2HPO_4, 1.9 g of 14 mM KH_2PO_4 dissolved in ddH_2O at 1L final volume. pH was adjusted to 7.4 with NaOH and stored at RT.

1X PBS with Ca/Mg: 10X PBS was diluted to 1X with ddH_2O. 0.1mM $CaCl_2$ and 1mM $MgCl_2$ were added.

100mM Glycine/ PBS-Ca-Mg: 375 mg of glycine was dissolved in 50 ml of PBS-Ca-Mg. The solution was freshly prepared and kept on ice.

Biotinylation Buffer: 10mM Triethanolamine, 2mM $CaCl_2$, 150mM NaCl were dissolved in ddH_2O, and pH was fixed to 7.5.

NHS-SS-Biotin Stock: (EZ-Link™ Sulfo-NHS-SS-Biotin, Thermo Scientific, cat no. 21331). 100 mg of Biotin was dissolved in 500 µl of DMSO to make a stock of 200 mg/ml. Biotin was aliquoted in 50 µl and wrapped in aluminium foil, stored at -20°C.

Biotin was diluted with biotinylation buffer to a final concentration of 1.25 mg/ml and kept on ice before the experiment.

Cell Lysis Buffer: 1% Triton X-100, 150mM NaCl, 5mM EDTA, 50mM Tris (pH 7.5) were mixed with ddH_2O and supplemented with 1X Roche protease inhibitor cocktail, 1mM Na_3VO_4 and 1mM PMSF before use and kept on ice.

Immunoprecipitation (IP) Buffer: 150mM NaCl, 50mM Tris (pH 7.5), 5mM EDTA, 0.5% Triton X-100 were mixed with ddH_2O and supplemented with 2mM Na_3VO_4, 2mM PMSF, 2x Roche protease inhibitor cocktail before use and kept on ice.

10X Roche protease inhibitor cocktail: One tablet of Roche protease inhibitor cocktail was dissolved in 1 ml of ddH_2O and store at -20°C.

Na_3VO_4 stock: Stock concentration of 100 mM was prepared in ddH_2O and kept at -20°C.

PMSF stock: Stock concentration of 100mM was prepared in EtOH and kept at -20°C.

Wash Buffers for Streptavidin/Agarose Beads:

1.Lysis Buffer: 1% Triton X-100, 150mM NaCl, 5mM EDTA, 50mM Tris were mixed and pH was adjusted to 7.5.

2.High salt wash buffer: 0.1% Triton X-100, 500mM NaCl, 5mM EDTA, 50mM Tris were mixed and pH was adjusted to 7.5.

3.No salt wash buffer: 50mM Tris was prepared in ddH_2O and pH was adjusted to 7.5.

3.2 METHODS

3.2.1 Cell Culture Maintenance

Three different cell lines were used for cell culture studies. All cell lines were purchased from ATCC and were grown according to ATCC directions. All cells were grown in incubator with 5% CO_2 at 37°C at ambient air. H9c2 (Rat Ventricular Cardiomyocytes) cell line was used for this project. H9c2 cells were cultured in complete DMEM (cDMEM) containing 1000mg/L glucose, 4mM L-glutamine, 1mM Na-pyruvate, 1X Penicillin-Streptomycin, 5mM HEPES and 10% fetal bovine serum (FBS). The medium was replaced every two days. H9c2 cells were grown until the confluency reached to 80%.

Cell harvesting: Medium of the cells was aspirated and 5 ml PBS was added. Then, 3 ml PBS-EDTA-Trypsin was added, and cells were incubated for 2-3 min at 37°C. For inhibiting PBS-EDTA-Trypsin activation, 7 ml cDMEM was added and centrifuged at 500rpm for 5 min. Cells were seeded in T75 cell culture flask with the desired splitting ratio (1:4-1:5) and were seeded to various cell culture flasks or dishes at 10.000cell/cm^2 seeding density.

Amplification of shHIF-1α containing adenoviruses: Adenoviruses expressing GFP shHIF-1α and a scrambled sequence against rat genome have been generated and used in our previous studies (54). In this study, we amplified the adenoviruses to obtain high viral titres. For these studies, HEK293T (Human Embryonic Kidney, from ATCC) cell line was used. HEK293T cells were maintained in T75 cell culture flasks with 4500g/L glucose cDMEM (500 ml) containing 5 ml pen/strep (100X), 5 ml HEPES (1M), 5 ml L-glutamine (100X), 50 ml FBS, 500 µl sodium pyruvate (1mM). HEK293 cells were seeded on 1:50 diluted (in PBS) rat tail type V collagen coated 10cm petri dishes and passaged at 1:10 splitting ratio.

For these studies, cells were seeded on rat tail type V collagen coated T75 cell culture flasks. Next days, cells were infected with 1MOI (multiplicity of infection) adenovirus particle per cell. When all cells detached from the surface of the flasks, the medium containing the virus was collected in falcons and centrifuged at 2000g for 5 min at 4°C. The supernatant was removed and 2 ml of DMEM was added to the cell

pellet, vortexed, frozen, and thawed three times to release the adenovirus from the cells. After final thawing, tubes were centrifuged two times at 5000g for 10 min to pellet unbroken cells and nuclei. Supernatants were collected and mixed with equal volume of sterile 50% glycerol. Adenoviruses were aliquoted and stored at -80°C.

The titres of adenoviruses have been calculated according to End-Point Dilution Assay. For this, 10^5 HEK293 cells were seeded on collagen coated 12 well plates in 0.5 ml medium. When all cells attached, medium was removed, and fresh medium was added. The viruses prepared at different dilution ratios were given to the cells. About 24h later, cells were examined under a fluorescent microscope for GFP expression. Virus titters were calculated according to the formula:

MOI/ml=original dilution x cell density x final dilution x 2,5 x % shining cell.

In addition, HEK293FT (Human Embryonic Kidney) cell line was used for lentivirus production because of high transfection efficiency. HEK293FT cells were maintained with cDMEM in the 10cm petri dishes. For the cDMEM, 5ml pen/strep (100X), 12.5 ml HEPES (1M), 5 ml MEM NEAA (100X), 5 ml L-glutamine (100X), 50 ml FBS, 500 µl MEM sodium pyruvate (1mM) were added into DMEM. HEK293FT cells were passaged 1:10 or 1:20 splitting ratio.

3.2.1.1 Cell Counting and Freezing

Cells were collected into falcon as in passaging and 30 µl of cell suspension was mixed with 30 µl of trypan blue dye. From this mixture, 10 µl was loaded into the hemacytometer and counted. Cells were centrifuged at 500rpm for 5 minutes. Supernatant was removed and 2×10^5 cells were resuspended with 1 ml cell freezing medium and kept in cryovials, stored at -80°C in Mr. Frosty box for 48 hours. Then, cryovials were stored in liquid nitrogen tank for long-term storage.

3.2.1.2 Cell Thawing

Cells were taken from the liquid nitrogen tank and thawed in 37°C water bath approximately for 1 min and were added into 9 ml cDMEM, centrifuged at 500rpm for 5 min and medium was aspirated. Cells were seeded in T25 cell culture flasks and kept in regular CO_2 incubator at 37ºC.

3.2.2 In-Vitro Hypoxia

To mimic ischemic heart disease model an oxygen-level adjustable CO_2 incubator (Binder) was used. Cells were exposed to hypoxia at 1%O_2 for 24 hours at 37°C. For normoxia conditions, cells were kept in regular CO_2 incubator (~19%O_2) at 37°C for 24 hours.

3.2.3 HIF-1α Gene Expression Silencing Experiments

H9c2 cells were seeded into 10cm cell culture dishes in 8 ml cDMEM at $6x10^5$ cell density. Next day, cells were infected with adenoviruses containing scr.vir.co. (scrambled virus control) and shHIF-1α in 10% FBS medium without antibiotics as 100MOI/cell. After 24 hours, viruses were removed from the dishes and cDMEM was added. Cells were incubated in normoxia (~19%O_2) and hypoxia (1%O_2) for 24h and used for the experiments.

3.2.3.1 Whole Cell Lysate Preparation

Cells were washed three times with cold PBS and scraped from dishes in 300 µl lysate buffer. Lysates were incubated at 4°C for 20 minutes and vortexed every 5 min, centrifuged at 10000g for 10 min at 4°C and supernatants containing whole cell lysates were kept in separate microcentrifuge tubes. Concentration of proteins were measured with Bradford assay (Bio-Rad) and stored at -80°C until use.

3.2.3.2 SDS-PAGE and Western-Blot

The SDS (sodium dodecyl sulfate) gel consisted of resolving (10%) and stacking sections (4%). Resolving and stacking content is shown in table 2 and table 3. For SDS-PAGE and western blot experiments, 20µg of total protein was used. The gels were run at 80 V with 1X running buffer until the samples passed the stacking part, then increased to 110 V. Wet blotting was performed at 65 V for 90 minutes at 4°C. The efficiency of the blotting was confirmed by Ponceau staining and membranes were blocked with 5% BSA-TBST for 30 min, and then incubated with the appropriate primary antibodies (HIF-1α: Cell Signaling, rabbit, cat no: D2U3T; β-actin: Sigma, mouse, cat no: A2258; α1 NKA: Abcam, mouse, cat no: ab7671) overnight at 4°C. Next day, after washing with Tris buffered saline containing 0.1% Tween-20 (TBST), membranes were incubated with horse-radish peroxidase (HRP)-coupled secondary antibodies (anti-rabbit: Calbiochem, cat no: DC03L; anti-mouse: GE Healthcare, cat no: NXA931) for 1 hour at RT. The membranes were washed again with TBST, and they were incubated with enhanced chemiluminescence (ECL) solution and imaged with ChemiDoc Imaging System. Band densities have been normalized to β-actin band densities.

Table 2: The recipe of resolving gel (lower) for SDS-PAGE.

Resolving Gel	**10%**	
	2 gels	4 gels
Volume (ml)	15	30
ddH_2O	4,12	8,23
RGB	3,75	7,50
10 % SDS	0,15	0,30
30 %Acrylamide	4,87	9,74
2% Bis-acrylamide	1,95	3,90
10 % APS	0,150	0,300
Temed	0,015	0,030

Table 3: The recipe of stacking gel (upper) for SDS-PAGE.

Stacking Gel	**4%**	
	2 gels	4 gels
Volume (ml)	7,5	15
ddH_2O	4,09	8,18
SGB	1,89	3,78
10 % SDS	0,08	0,15
30 %Acrylamide	0,97	1,95
2% Bis-acrylamide	0,39	0,78
10 % APS	0,075	0,150
Temed	0,0075	0,015

3.2.3.3 Immunofluorescence (IF) Experiments

H9c2 cells were seeded on 8 well cover slips (Ibidi) at a density of 2×10^3 cells/ well. After 24 hours, cells were infected with scr.vir.co. or shHIF-1α adenoviruses in 10% FBS medium without antibiotics as 100MOI/cell. Next day, viruses were removed, cDMEM was added on each well and cover slips were incubated in normoxia (~19%O_2) or hypoxia (1%O_2) for 24h. Next day, cells were washed three times with sterile cold phosphate buffered saline (PBS) containing $CaCl_2$, $MgCl_2$ (PBS-Ca-Mg) and they were fixed with -20°C methanol for 5 min at RT. Cells were washed three times with sterile PBS and PBS containing 0.1% Tween-20 (PBST) was added on each well for 5 min for permeabilization. Blocking was performed with 5%BSA+PBST for 30 min at RT and cells received HIF-1α rabbit primary antibody at a dilution of 1:1000 prepared in 1% BSA+PBST. Next day, cells were washed four times with sterile PBS and incubated with secondary antibody (Alexa Flour Plus 555 goat anti-rabbit, Thermo Scientific) at a dilution of 1:1000 in 1% BSA+PBS for 1 hours at RT in the dark. Cells were washed with PBS four times for 5 min in the dark. Mounting solution containing DAPI was added on each well and cover slips were imaged by confocal microscope with 63X oil objective (Carl Zeiss, LSM700).

3.2.4 Cell Surface Biotinylation Experiments

Cell surface biotinylation assay was performed to identify the expression of α1 NKA at the cell membrane. For these experiments EZ-Link™ Sulfo-NHS-SS-Biotin (Thermo Scientific) which does not penetrate the cells, and which reacts with primary amino groups (-NH2) of the proteins at the cell surface was used. H9c2 cells exposed to normoxia or hypoxia for the indicated times were kept on ice, medium was aspirated, cells were washed three times with 3 ml PBS-Ca-Mg. For 10cm dishes NHS-SS-Biotin at a final concentration of 1.25 µg/ml was added. Plates were incubated on ice for 20 min on a shaker protected from light. Plates were washed three times with 3 ml 100mM Glycine in PBS-Ca-Mg and incubated for 10 min during each wash. Plates were washed once with PBS-Ca-Mg for 10 min and then 200 µl cell lysis buffer was added. Whole cell lysates were prepared as described above. Protein levels of the lysates were measured with Bradford assay.

Two hundred microgram (200ug) of total whole cell lysates were mixed with 100µl of Streptavidin Agarose Resins (Pierce, Thermo Scientific) which specifically binds to biotin and tubes were rotated overnight at 4°C. Next day, beads were centrifuged at 12000rpm for 2 min at 4°C. Supernatants (150µl) containing non-biotinylated proteins were considered cytoplasmic fractions, were kept in separate tubes. Rest of the samples were aspirated without destroying the beads, and they were washed two times with 400 µl of high salt, three times no salt wash buffer and once with 50mM Tris (pH 7.5) and they were centrifuged at 10000rpm for 2 min.

Finally, 25 µl of 4X Laemmli sample buffer supplemented with 10% mercaptoethanol was added on the beads. In parallel equal volume of supernatants containing cytoplasmic fractions were also mixed with 2X Laemmli sample buffer. Denaturation was performed at 37°C for 30 min, tubes were kept on ice, vortexed and spun down at 17000g for 2 min. Equal volume of samples were loaded on 10%SDS-PAGE. Membrane and cytoplasmic expression of α1 NKA was measured by Western Blot. The expression of β-actin was also measured for loading control and to check the purity of the membrane fraction. The existence of β-actin expression in cytoplasmic fractions but not in membrane fractions has been considered successful pure membrane preparation.

3.2.5 Immunoprecipitation (IP) Experiments

To analyse proteins that interact with α1 NKA subunit with proteomic analysis, immunoprecipitation experiments were performed. Since these experiments are carried out first time, optimization studies were performed (data are given in the result section Figures 10-11). These experiments included different amount of total protein, Protein A Agarose beads, composition and concentrations of the detergents and protease inhibitor cocktail in the cell lysis buffer. Based on optimization studies, the final version of the IP protocol used for proteomic studies is given below.

Whole cell lysates from normoxic or hypoxic HIF-1α silenced and control cells were prepared as discussed above, and they were freshly used for the experiments. Protein A Agarose beads (Praesto Jetted A50, Purolite) were centrifuged at 500g for 30 sec at 4°C. Supernatant was discarded and a volume of sterile PBS-Ca-Mg equal to the bead volume was added, centrifuged at the same speed again. Beads were washed with PBS three times. After the final wash with PBS, the beads were washed once with cell lysate buffer (LB) and spun down. A volume of immunoprecipitation lysate buffer (IP-LB) equal to the bead volume was added to obtain 50% Protein A Agarose beads.

To eliminate non-specific binding, a pre-cleaning step was introduced. About 600 ~µg total whole cell lysate from each treatment was mixed with 100 µl Protein A Agarose beads. The total volume was adjusted to 500 µl with LB, and gently rotated at 10 rpm for 30 min at 4°C. Mixtures were centrifuged at 1000g for 2 min at 4°C and the supernatants were collected in separate microcentrifuge tubes.

Pre-cleaned lysates were mixed with 6µg of primary antibody specific to α1 NKA (Abcam, mouse, cat no: ab7671) or 6µg Mouse IgG antibody (Cell Signaling, cat no: 5415) as isotype control, incubated for 30 min at 4°C to allow the antibody binding to proteins. Then, 250 µl Protein A Agarose beads were added, total volume was adjusted to 750 µl with LB. Bead control and cell lysate with no antibody was also included. The samples were gently mixed for 2,5 hours at 10 rpm at 4°C and they were centrifuged at 2000g for 2 min at 4°C. Supernatants were collected in separate microcentrifuge tubes and beads were washed two times with 750 µl of LB without protease inhibitor cocktail. Beads were washed with a solution containing only 150mM NaCl and 50mM Tris (pH.7.5) and they were centrifuged at 2000g for 2 min at 4°C.

The supernatant fractions from each wash step were collected in separate tubes to determine the efficiency of IP by SDS-PAGE and Western Blot.

Proteins interacting with α1 NKA were eluted by 500 µl 0.1 M Glycine (pH:2-3) added to the bead pellets and mixed vigorously for 5 min at RT, centrifugated at 2000g for 2 min. Supernatants from the first elution step were called as E1 fraction. This process was repeated, this time centrifugation was performed at 5000g for 2 min and the 2nd elution fraction was obtained (E2). The pH of the elution fractions was neutralized to pH 7.0 using 125 µl Tris (1M). The efficiency of IP was examined by SDS-PAGE and Western Blot as mentioned above.

3.2.6 Identification of Partners of α1 NKA by Proteomic Studies

To identify the protein interacting partners of α1 NKA by hypoxia and HIF-1α, proteomic studies have been performed at TUBITAK-UME from IP samples. Briefly, protein levels from the IP elution fractions of antibody control (empty bead) and α1 NKA antibody received samples have been measured by QubitTM Protein Assay and peptides have been acquired by FASP Protein Digestion Kit (Expedeon) according to manufacturer's protocols. Disulphide bonds of the proteins have been cleaved and samples were washed with urea and ammonium carbonate solutions. Peptides have been separated by reverse phase NanoLC liquid chromatography before mass spectrometer analysis. Thermo Scientific ™ UltiMate ™ 3000 RSLC Ultra Nano ultra-performance liquid chromatography and Thermo Scientific Q Exactive ™ HF mass spectrometry was used for the analysis. Analysis of the mass data has been performed with TraceFinder ™ and Proteome Discoverer 2.4 softwares based on NCBI Rattus Norvegicus (Rat) (Taxonomy No: 10116).

3.2.6.1 Comparative Group Analysis

For the quantitative and comparative analysis in the interactomes Proteome Discoverer 2.4 has been used. Each elution fraction has been analysed three times and peptides identified at least in two analyses have been included to minimize the technical false negative results. Identified proteins in the treatment sets were compared

as different groups and comparative analyses between groups have been performed on raw data. Bead:sample ratio has been kept 0.5 to exclude non-specific results. Experiments and analysis have been performed from three independent IP preparations.

3.2.6.2 Bioinformatics Analysis

The abundance ratio and coverage parameters obtained from mass spectroscopy were analyzed with the Cytoscape software (55). Functional enrichment analysis was performed on Atp1α1 interactomes via STRING DB. False Discovery Rate (FDR) <0.05 has been considered significant.

3.2.7 Generation of HIF-1α Knock Out H9c2 Cells by CRISPR/Cas9 System

3.2.7.1 sgRNA and Primer Design

To generate HIF-1α knockout H9c2 cell line by CRISPR/Cas9 gene editing technology, HIF-1α transcripts in Rattus Norvegicus were examined in database (Ensemble) and transcript HIF-1α-201 was selected (56). Two different sgRNAs were designed using CRISPOR (crispor.tefor.net) online tool. Oligos of designed sgRNAs showed in Table 4.

Gene: Hif1a ENSRNOG00000008292

Description	hypoxia inducible factor 1 subunit alpha [Source:RGD Symbol;Acc:61928]
Gene Synonyms	MOP1
Location	Primary_assembly 6: 92,624,390-92,669,261 forward strand. mRatBN7.2:CM026979.1
About this gene	This gene has 1 transcript (splice variant), 229 orthologues, 7 paralogues and is associated with 102 phenotypes.
Transcripts	Hide transcript table

Show/hide columns | Filter

Transcript ID	Name	bp	Protein	Translation ID	Biotype	UniProt Match	Flags
ENSRNOT00000049725.4	Hif1a-201	3700	826aa	ENSRNOP00000042230.4	Protein coding	D4A8P8	APPRIS P1

Figure 5: Rat HIF-1α transcript list. There is 1 transcript of HIF-1α of Rat (56).

Table 4: The list of CRISPR oligos and sequences.

Names of Oligos	Sequences of Oligos
HIF-1αCrispr1top	CACCGTTGATAAAGCTTCTGTTATG
HIF-1αCrispr1bot	AAACCATAACAGAAGCTTTATCAAC
HIF-1αCrispr2top	CACCGATAACGTGAACAAATACAT
HIF-1αCrispr2bot	AAACATGTATTTGTTCACGTTATC

3.2.7.2 Annealing of sgRNA Oligos

Complementary top and bottom HIF-1α-CRISPR1, HIF-1α-CRISPR2 oligos were annealed according to the protocol given in Table 5 and the reaction conditions given in Table 6.

Table 5: List of annealing reaction components.

Components	Volume (µl)	Final Concentration
Top oligo (100µM)	1 µl	10µM
Bottom oligo (100µM)	1 µl	10µM
T4 Ligation Buffer (10X)	1 µl	1X
T4 PNK (10U/µl)	1 µl	1U/µl
ddH_20	6 µl	
Total	10 µl	

Table 6: Annealing reaction conditions carried out on T100™Thermal Cycler.

Temperature(ºC)	Time Point
37ºC	30 min
95ºC	5 min
95ºC to 25 ºC	Ramp down
+4ºC	∞

Top and bottom oligos of sgRNA were used as control. Annealed oligos and control were run on a 2% agarose gel at 90V for 30 min to see the efficiency of annealing. Bands were imaged with ChemiDoc Imaging System.

3.2.7.3 Golden Gate Ligation Reaction

Annealed HIF-1α oligos were cloned into a LentiCRISPR v2 plasmid, which was digested by the Esp3I. This experiment was carried out according to the protocol given in Table 7 and the reaction conditions given in Table 8.

Table 7: Golden gate ligation reaction components.

Components	**Volume (µl)**
LentiCRISPR v2 (25 ng/µl)	1 µl
Annealed sgRNAs (1:100)	1 µl
Cut Smart Buffer (10X)	2 µl
ATP (10 mM)	2 µl
Esp3I	0,5 µl
T4 DNA Ligase (400 U/µl)	0,5 µl
ddH_2O	13 µl
Total	20 µl

Table 8: Golden gate ligation reaction conditions.

Temperature (ºC)	**Time Point**
37ºC	5 min
20ºC	5 min- **15X**
+4ºC	∞

3.2.7.4 Transformation

Cloned plasmids were transformed into 200 µl of E. coli NEB-Stable competent cells. From ligation reactions 10 µl were mixed with the competent cells and were kept on ice for 30 min. Mixtures were kept at 42ºC for 90 sec to heat shock and were kept on ice for 1 min. Then, 800 µl LB was added to each tube and they were incubated at 37ºC for 45 min. Mixtures were centrifuged at 13000rpm for 30 sec, 900 µl supernatant was discarded from each tube and pellets were resuspended with remaining 100 µl LB. Glass beads were spread on the LB agar plates and mixed with cell suspensions. These plates were incubated at 37ºC for 16 hours. In addition, replication plate was prepared using colonies observed at the end of 16 hours.

3.2.7.5 Colony PCR

After the transformation of HIF-1α sgRNAs cloned into appropriate bacteria, growing colonies were randomly selected to check if they have taken the insert with colony PCR. For this purpose, a forward primer that fits the U6 promoter region located on the plasmid backbone and a reverse primer that fits the bottom oligo of the guide RNA were used. The expected DNA length of this PCR reaction is 276 base pairs. Ten colonies were selected and sketched on the LB agar replica plates. Rest of the material was kept in PCR reaction tubes respectively. In addition, no insert and no template reactions were used as control. PCR reactions were performed according to protocol given in Table 9 and the reaction conditions given in Table 10.

Human U6 forward primer (GAGGGCCTATTTCCCATGATTCC) as forward primer and bottom oligos of each sgRNA as reverse primers were used in colony PCR.

Table 9: Colony PCR reaction components.

Components	Volume (µl)
Mg^+ free standard tag buffer (10X)	1,25 µl
$MgCl_2$ (25 mM)	0,65 µl
dNTP (10mM)	0,2 µl
Forward primer (10 µM)	1 µl
Reverse primer (10 µM)	1 µl
Tag DNA polymerase	0,125 µl
ddH_2O	5,775 µl
Total	10 µl

Table 10: Colony PCR conditions.

Temperature (ºC)	Time Point
95ºC	3 min
95ºC	30 sec
54ºC	30 sec
68ºC	30 sec 28 X (Step 2)
68ºC	5 min
+4ºC	∞

The products of the colony PCR were run on the 1% agarose gel at 100V for 1 hours. Bands were imaged with ChemiDoc Imaging System. Furthermore, three colony products with an expected length of 276 bp were selected from replica plate and selected colonies were grown in liquid bacterial cell culture at 37ºC for 16 hours to amplify for miniprep plasmid isolation.

3.2.7.6 Isolation of Plasmids with Alkaline Lysis Solution

After 16 hours, 885 µl grown bacteria and 115 µl 87% glycerol were mixed into a tube and stored at -80ºC. For the plasmid isolation, 1.5 ml of grown bacteria were added into microcentrifuge tubes and centrifuged at 17000g for 30 sec. Supernatants were removed and 100 µl alkaline lysis solution I (AI) solution was added, and pellets were resuspended. Then, 200 µl of freshly prepared alkaline lysis solution II (AII) was added, tubes were inverted and 150 µl alkaline lysis solution III (AIII) was added. Tubes were incubated on ice for 4 min and centrifuged at 17000g for 5 min. Supernatants were transferred into new tubes and kept on ice. Absolute ethanol was added 2-fold volume of supernatants and centrifuged at 17000g for 5 min at 4ºC. Supernatants were aspirated and tubes were kept on the ice, 1 ml of 70% EtOH was added on the pellets. Centrifugation was performed at 17000g for 2 min at 4ºC, supernatants were removed, and pellets were air dried for 8 min. Pellets were resuspended with 50 µl TE buffer and RNase mixture, vortexed and spun down. Isolated plasmids were stored at -20ºC.

3.2.7.7 Sanger Sequencing

Sanger sequencing was performed for confirmation of sgRNA sequences cloned into plasmids using U6 primer (GAGGGCCTATTTCCCATGATTCC). This procedure was done by the MEDSANTEK (http://www.medsantek.com.tr/). One pair reading was performed, and Sanger sequencing results were analysed using Snap Gene Viewer 5.2.4.

3.2.7.8 Plasmid Preparation for Transfection

pMDLg/pRRE, pRSV-Rev, pCMV-VSV-G and LegoG2-Puro plasmids were gifts from Dr. Emre Deniz, Acibadem University. The plasmids were transformed into NEB Stable competent cells and intact colonies were selected. They were grown in liquid bacterial cell culture including the 3 ml LB broth with Ampicillin at 37ºC for 7 hours by shaking at 230rpm. After 7 hours, colonies were grown in 200 ml LB broth

with Amp at 37ºC for 16 hours by shaking at 230rpm for midiprep plasmid purification.

3.2.7.9 Midiprep Plasmid Isolation

Plasmid DNA of each chosen colonies were isolated using the PureLink® HiPure Midiprep Plasmid DNA Purification Kit (Invitrogen) according to manufacturer's instructions.

3.2.7.10 Control Digestion

Plasmids used for transfection were verified by restriction enzyme digestion. The enzymes and enzyme specific buffers used in this experiment are given in Table 11. Control digestion was performed according to protocol given in Table 12 and the reaction conditions given in Table 13.

Table 11: List of used enzymes and buffers

Name of Enzymes	Name of Buffers
EcoRI-HF	Cut Smart Buffer (10X)
HindIII-HF	Cut Smart Buffer (10X)
SacI	SacI Buffer (10X)

Table 12: Control digestion components.

Components	Volume (µl)
Enzyme	1 µl
DNA	1 µg
Buffer	5 µl
ddH_2O	Up to 50 µl
Total	50 µl

Table 13: Control digestion reaction conditions.

Temperature (ºC)	Time Point
37ºC	2 hours
+4ºC	∞

PCR products of control digestion were run on the 1% agarose gel at 100V for 90 min. Bands were visualized with ChemiDoc Imaging System.

3.2.7.11 2X HBS Transfection

For each sample, $3x10^6$ HEK293FT cells were seeded on 0.1% gelatine coated 10cm cell culture dishes. Next day, medium was changed with the cDMEM with 5% FBS and containing 25 µM chloroquine. After 2 hours, for 3rd generation lentivirus production, 3750 ng pMDLg/pRRE, 2250 ng pRSV-Rev, 1500 ng pCMV-VSV-G were separately mixed with 7500 ng LentiCRISPR v2 in 120 µl of 1M $CaCl_2$ and volumes were completed 500 µl with ddH_2O. While vortexing, 500 µl of 2X HBS was added dropwise to the mixtures and mixtures were incubated at RT for 15 min. These mixtures were dropped on the cells. pcDNA-GFP used as a control for transfection. Next day, the medium was changed. At 24th and 48th hours, medium containing lentiviruses were collected, filtered through 0.44 µm filter and stored at -80°C.

3.2.7.12. MTT Assay

MTT colorimetric assay was performed to determine the cell viability after treatment with Puromycin. H9c2 cells ($2x10^3$) were seeded into 96 well cell culture plate in 100 µl medium. After 24 hours, different concentrations of Puromycin were added for 24, 48 and 72 hours. At the end of the treatment, 10 µl MTT reagent ((3-(4,5-Dimethylthiazol-2-yl)-2,5-Diphenyltetrazolium Bromide) were added into each well and cells were incubated 4 hours at 37°C. MTT dye enter the living cells and dark blue formazan is produced when live cells split the yellow substrate MTT. Four hours later, cells were washed with 100 µl PBS and 100 µl MTT solvent buffer was added. MTT solvent (consist of 10mM HCl, 0.2% Nonidet P40, Isopropanol and 50% DMSO) added as blank. Plate was shaken for 10 min, and absorbance was measured with spectrophotometer at 595 nm. Blank values were subtracted from absolute absorbance readings and half maximal inhibitory concentration (IC50) of Puromycin obtained from dose response curves was calculated by non-linear regression for the best fit using SigmaPlot v10.

3.2.7.13 Infection of H9c2 cells with CRISPR/Cas9 Carrying Lentivirus

H9c2 cells were seeded into T25 cell culture flasks in 5 ml cDMEM as 10^5 cells per flask. Next day, medium was aspirated and 4 ml lentivirus containing 8 µg/ml protamine sulphate at final concentration was added on the cells. Medium was aspirated after 16 hours and cDMEM was given. Next day, medium was replaced with 5 ml medium containing 0,4 µg/ml Puromycin for selection. In addition, Lego G2 infected cells were used as infection control. While maintaining the cells they were passaged regularly and $2x10^5$ cells were saved for gDNA extraction during the Puromycin selection.

3.2.7.14 Deleting HIF-1α from H9c2 Genome

To delete the entire HIF-1α gene from the genome of H9c2 cells, cells were co-transfected with both HIF-1α-CRISPR1 and HIF-1α-CRISPR2. To obtain HIF-1α KO homozygous cell line, cells were seeded in 96 well cell culture plates, one cell per well.

Also, non-target cells were used as control. Single cell colonies were selected with Puromycin. Growing cells were taken into 24 well cell culture plates, 6 well cell culture plates and T25 flasks, respectively. For screening of KO efficiency, cells were collected for genomic DNA isolation. My-Taq PCR was performed using isolated genomic DNA to check whether homozygous cells were obtained.

3.2.8 Determination the Efficiency of Genome Modification

3.2.8.1 Genomic DNA isolation

The genomic DNA of HIF-1α KO cell pools were manually extracted using the Tails-Proteinase K procedure. Genomic DNA isolation was performed from $2x10^5$ cells. For each sample, 10 µl of Proteinase K (20 mg/µl) and 500 µl tail lysis buffer were mixed and from this mixture 500 µl was added on each pellet and incubated at 55ºC in heat block for 90 min. Then, 250 µl of 5M NaCl was added, and they were incubated on ice for 10 min, centrifuged at 3000rpm for 45 min at 4ºC. The supernatants were transferred into new microcentrifuge tubes and 650 µl isopropanol was added and incubated at RT for 15 min. Mixtures were centrifuged at 17000g for 10 min, supernatants were discarded and 70% EtOH was added on each pellet. Centrifugation was repeated at 17000g for 10 min. Pellets were dried at room air and suspended with 50 µl TE buffer and RNase A mixture, stored at 4°C.

3.2.8.2 On Target PCR optimization

To determine the genomic modification rate, T7E1 assay was performed. For T7E1 assay, modified genomic regions were amplified by PCR. For this purpose, forward and reverse primers were designed for each target region that were shown in Table 14. Primers were optimized at different temperatures. PCR reactions were performed according to protocol given in Table 15 and the reaction conditions given in Table 16. In addition, 5X Phusion Polymerase PCR reaction was performed for optimization of primers according to protocol given in Table 17 and reaction conditions given in Table 18.

Table 14: On target primers and sequences.

Name of Primers	Sequences of Primers
HIF-1αCrispr1PCRfwd	TCATCAGTTGCCACTTCCCC
HIF-1αCrispr1PCRrev	TTGGACACCAGCACCACATT
HIF-1αCrispr2PCRfwd	CCACATGTGCCCTTACAGGT
HIF-1αCrispr2PCRrev	TCACCATTTCTGTGTGTAAGCA

Table 15: Components of My-Taq Polymerase PCR reaction.

Components	Volume (µl)	Final Concentration
Template DNA	1 µl	
My-Taq Reaction Buffer (5X)	5 µl	1X
Forward Primer (2.5 µM)	2 µl	0.2 µM
Reverse Primer (2.5 µM)	2 µl	0.2 µM
My-Taq DNA Polymerase(5U/ µl)	0.5 µl	0.1 U/ µl
ddH_2O	14.5 µl	
Total	25 µl	

Table 16: Reaction conditions of My-Taq Polymerase PCR.

Temperature	Time
95°C	1 min
95°C	0.15 sec
Annealing Time	0.15 sec
72°C	0.18 sec
	30X
4°C	∞

Table 17: Components of 5X Phusion Polymerase PCR reaction.

Components	Volume (µl)
5X Phusion GC Buffer	4 µl
dNTP's (10mM)	0.4 µl
Forward Primer (10µM)	1 µl
Reverse Primer (10µM)	1 µl
gDNA	0.5 µl
Phusion DNA Polymerase	0.2 µl
ddH_2O	13.9 µl

Table 18: Reaction conditions of 5X Phusion Polymerase PCR.

Temperature	Time
98°C	30 sec
98°C	15 sec
Annealing TM	15 sec
72°C	18 sec **30X**
72°C	10 min
4°C	∞

Products of the PCR were run on the 1% agarose gel at 100V for 1 hours. Bands were imaged with ChemiDoc Imaging System.

3.2.8.3 T7E1 Assay

After the delivery of the CRISPR/Cas9 constructs into the cells, cells form heterogeneous population. Heterogeneity of populations were calculated by T7E1 assay that was performed using on target PCR products made with isolated genomic DNAs. For each sample, a reaction without T7 enzyme was used as control. Protocol of T7E1 assay given in Table 19.

Table 19: T7 Endonuclease 1 Assay components and conditions.

1.AnnealingReaction			
On-Target PCR product		10 µl	
1X NEB Buffer 2		2 µl	
ddH2O		7.5 µl	
2.AnnealingConditions			
Step	**Temperature**	**Ramp Rate**	**Time**
Initial Denaturation	95°C		5 min
Annealing	95°C - 85°C	-2°C/sec	
	85°C - 25°C	-0.1°C / sec	
Hold	4°C		Hold
3.T7Endonuclease 1 Treatment Reaction			
Annealed PCR		19.5 µl	
T7E1 Enzyme		0.5 µl	
4. Treatment Protocol			
Incubation	37°C		15 min

T7E1 products were run on the 2% agarose gel at 80V for 90 min. Bands were imaged with ChemiDoc Imaging System. Band densities were calculated with ChemiDoc software and modification rate calculation was performed according to the formula in figure 6.

$$fraction\ cleaved = \frac{cut\ bands}{(uncut\ band + cut\ bands\ )}$$

$$\%\ Modification = 1 - \sqrt[2]{1 - fraction\ cleaved}\ \times 100$$

Figure 6: Calculation formula for percent rate of modification percent according to T7E1 assay results (57).

3.2.8.4 Statistical Analysis

Data are shown as mean ± SD. Statistical analysis was performed by one-way ANOVA and pair-wise multiple comparison (LSD) tests using SigmaPlot v10 (Systat Inc., Erkrath, Germany). The level of statistical significance was $p < 0.05$. For the analysis of Western Blot band densities, Image J has been used. For bioinformatic

analysis free online String and Cytoscape software have been used. FDR<0.05 has been considered significant.

4. RESULTS

4.1. Silencing Efficiency of HIF-1α in H9c2 Cells by Adenoviruses

Silencing efficiency of HIF-1α in H9c2 cells, was tested in whole cell lysates obtained from normoxic, hypoxic and shHIF-1α infected cells as described in method section. Figure 7 shows that in scr.vir. infected control cells, HIF-1α protein expression increased by hypoxia (1%O_2, 24h) compared to normoxic cells. shHIF-1α totally inhibited increased HIF-1α expression in hypoxic cells, indicating that silencing efficiency is ~100% at the protein level.

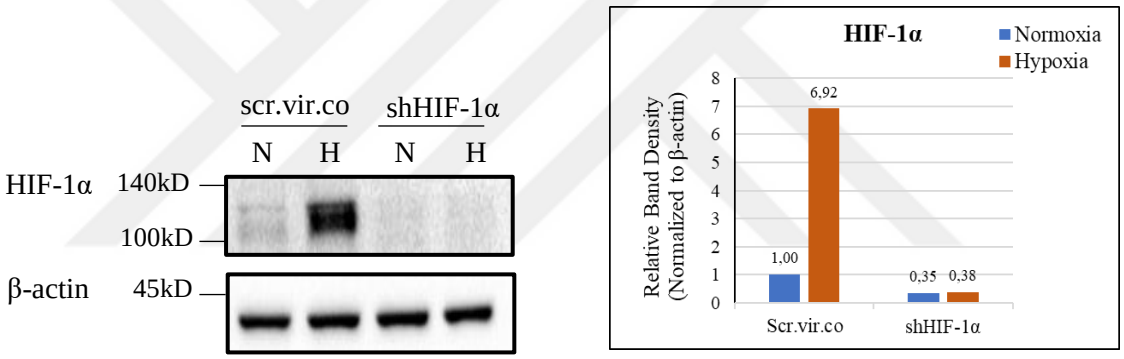

Figure 7: Efficiency of HIF-1α gene silencing in H9c2 cardiomyocytes. Protein expression of HIF-1α. Cells were infected with 100MOI of adenovirus for 24h and kept in normoxia (~19% O_2) or hypoxia (1% O_2, 24h). Band density of HIF-1α was normalized to β-actin band density.

We also performed immunofluorescence (IF) experiments to check intracellular localization of HIF-1α in normoxic, hypoxic and HIF-1α silenced cells. Figure 8 shows the representative confocal microscopy images. In normoxic cells, HIF-1α is expressed at the perinuclear area of the cells but not in the nucleus. In hypoxia, HIF-1α accumulated into nucleus and HIF-1α silencing in hypoxic cells completely abolished HIF-1α accumulation in the nucleus. These results were found to be compatible with the WB results.

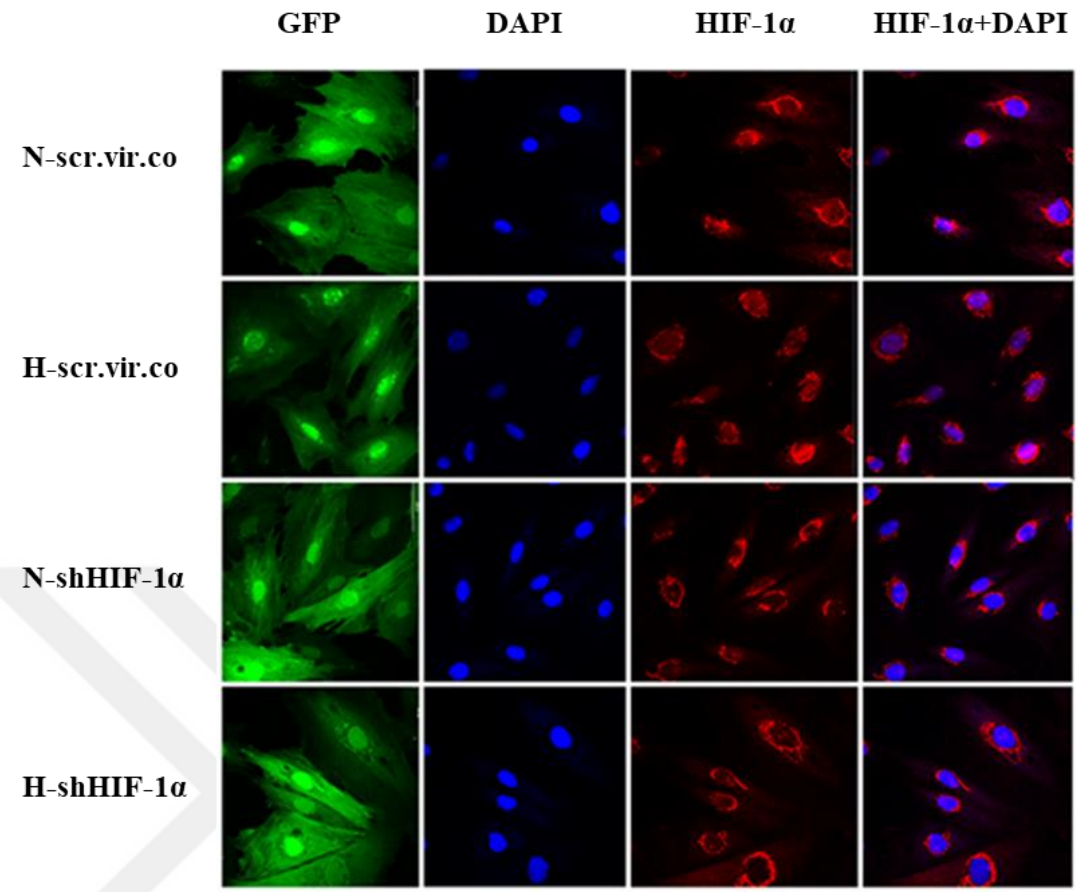

Figure 8: Confocal image of intracellular localization of HIF-1α in normoxic and hypoxic HIF-1α silenced cells. Cells were infected with 100MOI of adenovirus for 24h and kept in normoxia (19%O_2) or hypoxia (1%O_2). Immunofluorescence experiments have been performed using antirabbit secondary antibody against HIF-1α (AF 555 red) and DAPI for nuclear staining (against DNA) as described in Methods section. Images have been taken under 63X oil objective with Zeiss LSM700 confocal microscopy. N-scr.vir.co: normoxic cells received scr.vir.co. H-scr.vir.co: hypoxic cells received scr.vir.co. N-shHIF-1α: normoxic cells received shHIF-1α. H-shHIF-1α: hypoxic cells received shHIF-1α.

4.2. Investigating α1 NKA Expression by Cell Surface Biotinylation Experiments

In H9c2 cells, membrane expression of the α1 subunit of the Na^+/K^+-ATPase (α1NKA) pump decreased by 25% with hypoxia (p=0.003) and its internalization into the cell increased (p=0.004, Figure 9A, B). Silencing HIF-1α gene expression prevented the intracellular internalization of the α1 NKA in hypoxic cells (p=0.029). It is observed that in hypoxic + HIF-1α silenced cells membrane expression of α1 NKA

increased compared to hypoxic scr.vir.co cells which indicates increased translocation of α1 NKA to the membrane (p=0.004, 9A, B).

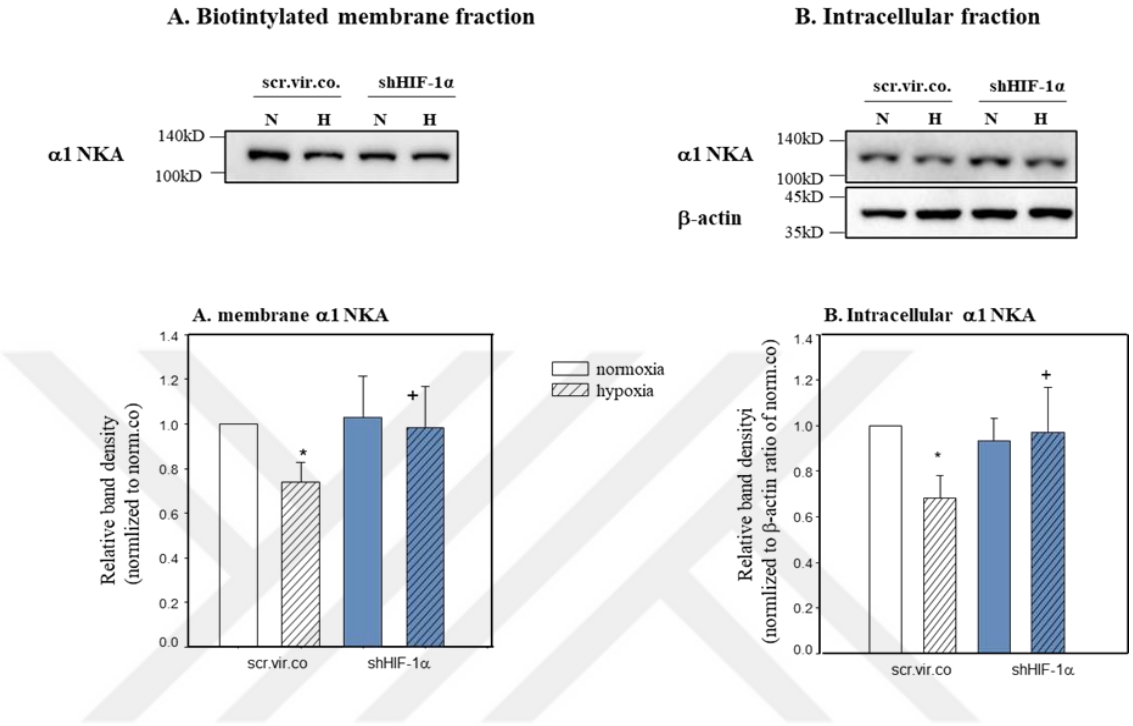

Figure 9: Effect of HIF-1α gene expression silencing on membrane and intracellular expression of the α1 NKA subunit in normoxic and hypoxic H9c2 cardiomyocytes. After cell surface biotinylation, 200µg total cell lysate from each sample was pulled down with streptavidin resin, protein expressions were investigated by Western Blot. Data given are normalized values of the band density of normoxic virus control and presented as mean ± SD of 4-6 independent experiments. Cell membrane expression of α1 NKA (A), intracellular expression of α1 NKA (B). *: Effect of hypoxia relative to normoxic control virus ; +: effect of gene expression silencing relative to hypoxic control virus $p < 0.05$.

4.3. Immunoprecipitation and Proteomic Studies

To understand about the regulation of α1 NKA in hypoxic and HIF-1α silenced cells in more detail immunoprecipitation (IP) and proteomic studies were carried out to identify the proteins interacting with the α1 NKA subunit that should provide the signalling pathways involved in this process.

IP experiments were performed from whole cell lysates of HIF-1α silenced and control H9c2 cells that were kept in normoxia or hypoxia. Since these experiments have been performed first time, we did optimization studies to test the efficiency of IP. In preliminary experiments we tested the amount of total protein, primary antibodies, Protein A Agarose beads needed for the assay (data not given). An antibody control that did not contain any primary antibody was always included as control sample. Based on these data, in a set of experiments, 200µg of total lysate protein, 2µg of α1 NKA and mouse isotype specific antibody and 100 µl of 50% Protein A Agarose beads were used for IP. General IP protocols, lysis buffers and assay conditions have been kept constant. Fractions obtained during washing steps and final elution fractions were run on two 10%SDS-PAGE followed by Western Blot as described in methods section. The efficiency of IP was tested by keeping one membrane directly in secondary antibody (Figure 10A) to see if IgG can be detected in the elution fractions by using HRP-coupled secondary antibody. Other membrane was incubated overnight in α1 NKA primary antibody (Figure 10B).

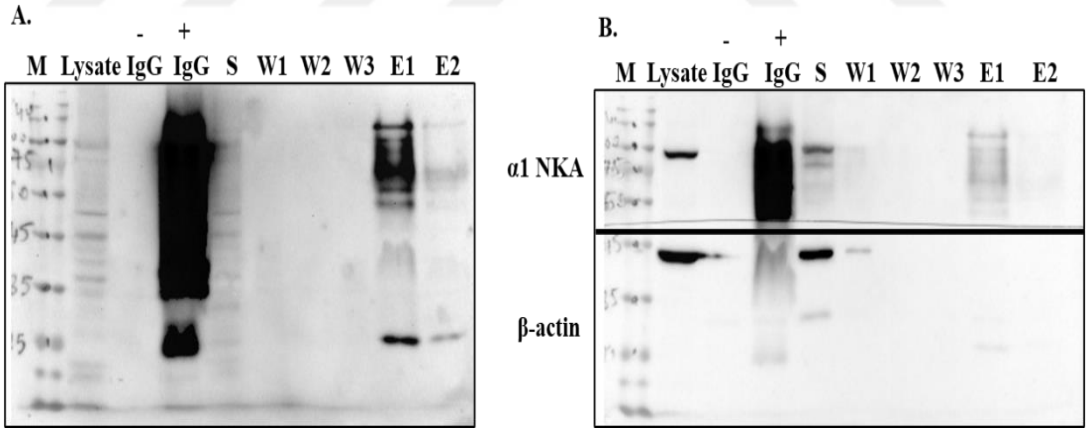

Figure 10: IP optimization experiment 1. Membrane was directly kept in HRP-coupled secondary antibody (A). Membrane was kept in primary antibody overnight (B). -IgG:beads without isotype specific mouse antibody, +IgG: beads with isotype specific mouse antibody, S: supernatant, W1: wash fraction 1, W2: wash fraction 2, E1: elution fraction 1, E2: elution fraction 2.

Based on this optimization study (Figure 10) we observed cleaved bands of α1 NKA and IgG from E1 fraction, though IP was considered successful. To decrease the cleavage of the proteins we increased the amount of lysate protein to 600µg, 250 µl Protein A Agarose bead, final concentration of protease inhibitor cocktail to 2x, and decreased Triton-X final concentration to 0.5% during IP for the next experiments. The efficiency of IP was evaluated on SDS-PAGE and Western Blot (Figure 11). Proteomic studies from the last optimization experiment have been tested and considered successful (data not given). We followed this established protocol for proteomic studies and tested the efficiency of IP on SDS-PAGE and Western Blot before the analysis (representative figure from IP experiments has been given at Figure 12).

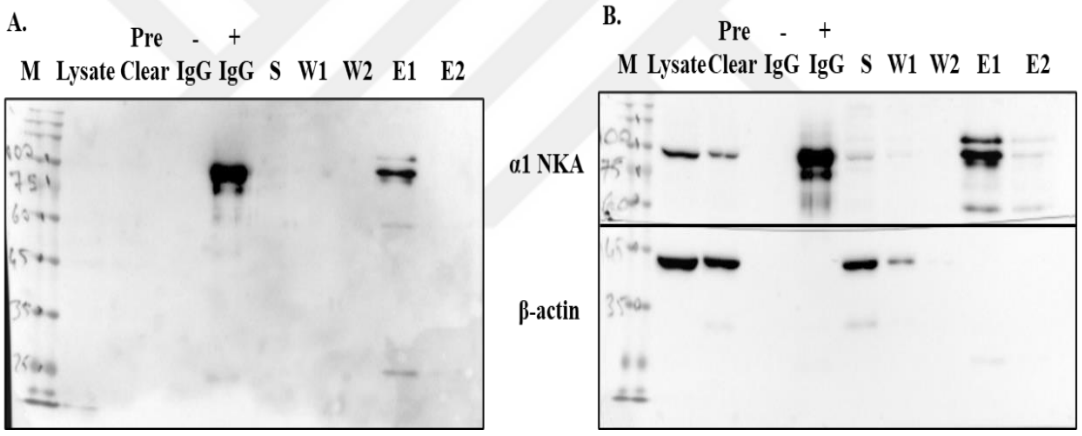

Figure 11: IP optimization experiment 2. Membrane was directly kept in HRP-coupled secondary antibody (A), membrane was kept in primary antibody overnight (B). -IgG: beads without isotype specific mouse antibody, +IgG: beads with isotype specific mouse antibody, S: supernatant, W1: wash fraction 1, W2: wash fraction 2, E1: elution fraction 1, E2: elution fraction 2.

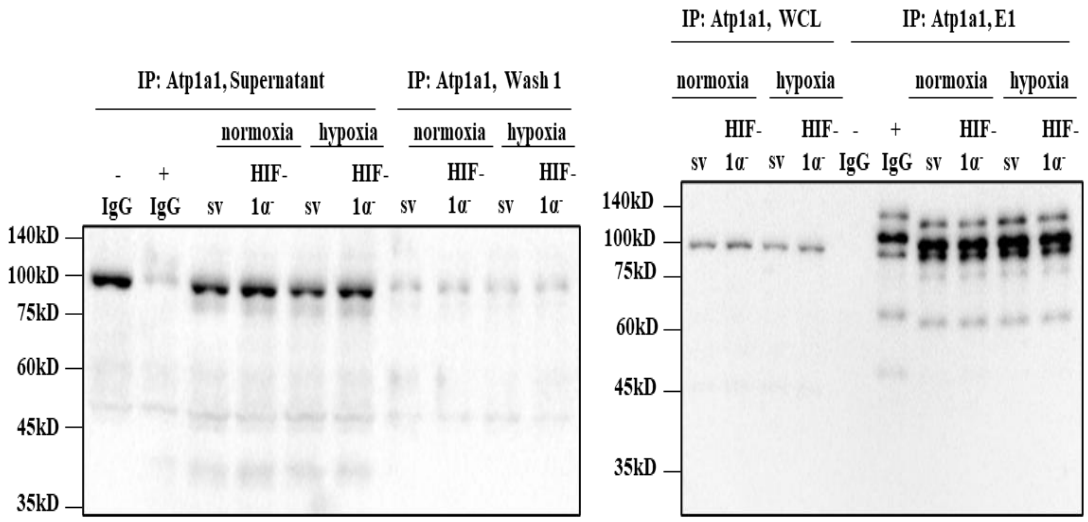

Figure 12: Western Blot image of representative α1 NKA immunoprecipitation experiment used for proteomic studies. Samples were separated in 10% gel. α1 NKA antibody was used for immunoblotting. -IgG: beads without isotype specific mouse antibody, +IgG: beads with isotype specific mouse antibody, S: supernatant, W1: wash fraction 1, WCL: whole cell lysate, E1: elution fraction

4.4 Identification of Protein Interacting Partners of α1 NKA by Bioinformatic Analysis

Bioinformatic studies identified that in normoxic and hypoxic cells α1 NKA non-specifically interacted with cell structure-cytoskeleton, muscle contraction-relaxation and focal adhesion associated proteins that were not affected by HIF-1α silencing. Total 53 specific interacting partners of α1 NKA have been identified (Table 20). Interactome analysis of α1 NKA also identified the interaction with β1 and β3 NKA that have been proposed to be involved in the membrane insertion of α1 NKA (21).

In hypoxic cells β1, β3 NKA abundance ratio decreased compared to normoxic cells; and HIF-1α silencing slightly increased the interaction. Also, in hypoxic cells abundance ratios of proteins involved in glycolysis and cell metabolism such as GAPDH, LDH, PKM increased, silencing HIF-1α abolished the interactions. Furthermore, α1 NKA interactome in hypoxic cells revealed increased abundance ratios with cytosolic chaperones heat shock protein Hsp1,5, Hsp90, Hsp47, Erp29, and

protein disulfide isomerase (PDI) which are related with endoplasmic reticulum (ER) homeostasis, found to be HIF-1α sensitive.

Among these interactions we identified Hsp47, an ER located protein acts as a chaperone in the biosynthetic pathway of collagen. Hsp47 directly binds to the luminal domain of inositol-requiring enzyme 1 (IRE1), facilitates its oligomerization in the adaptive phase of Unfolded Protein Response (UPR) that controls the faith of the proteins under stress conditions (58). Hypoxia increased α1 NKA-Hsp47 abundance ratio by 2.5-fold, and this interaction decreased to normoxic ratio in HIF-1α silenced hypoxic cells.

There was about 3-fold increased abundance ratio of Hsp90aa1, which is related with cellular stress responses, and it is involved in UPR in hypoxic cells. In HIF-1α silenced cells Hsp90aa1 interaction with α1 NKA decreased to normoxic ratio. Taken together, proteomic analysis revealed new protein interacting partners of α1 NKA in normoxic and hypoxic conditions that have not been reported in the literature previously, some of them being HIF-1α sensitive. Interaction network in hypoxic control and hypoxic HIF-1α silenced cells have been given in Figures 13 and 14 respectively. In addition, Venn diagram of α1 NKA interacting proteins has been given in Figure 15.

Reactome pathway analysis showed that cellular responses to stress increased in hypoxic control and HIF-1α silenced cells compared to normoxic HIF-1α silenced cells. HSF1 is a transcription factor activated by stress (59) and it is increased in hypoxia in HIF-1α sensitive manner. Similarly, calnexin/calreticulin cycle, Rho GTPase and heat stress pathways increased with hypoxia and decreased with silencing HIF-1α.

KEGG pathway analysis showed that pyruvate metabolism, HIF-1α signalling, glycolysis/gluconeogenesis, PI3K-Akt signalling, and RNA degradation pathways increased in hypoxia and decreased in hypoxic HIF-1α silenced cells. Proteins involved in cardiac muscle contraction increased in hypoxic control cells compared to normoxic HIF-1α silenced cells and it disappeared in hypoxic HIF-1α silenced cells.

Molecular function analysis showed that ubiquitin protein ligase binding increased with hypoxia and slightly decreased in normoxic HIF-1α silenced cells. Unfolded protein binding, protein disulfide isomerase activity and misfolded protein

binding were increased in hypoxic control cells. Protein kinase binding increased in hypoxic control cells, while decreased in normoxic HIF-1α silenced cells. Protein folding chaperone increased with hypoxia in HIF-1α sensitive manner. Kinase binding and anion binding increased in hypoxic control cells and disappeared with silencing HIF-1α.

In the cell, α1 NKA interacting proteins were mostly found at mitochondria, membrane bounded organelles, intracellular, endoplasmic reticulum, cytoplasm, and cytosol. Interacting proteins that only increased with hypoxia were resident at plasma membrane, extracellular region, lysosomes, secretory vesicles.

Table 20: Specific interacting partners of α1 NKA in normoxic, hypoxic, HIF-1α silenced cells or not.
NH1: normoxic HIF-1α silenced cells, HSV: hypoxic control cells, HH1: hypoxic HIF-1α silenced cells,

		Abundance ratio of NSV		
	Gene name	**NH1**	**HSV**	**HH1**
norm shHIF-1α	Mfge8	1,480	0,819	1,142
	Capzb	1,620	0,897	1,175
	Klhl22	1,841	1,155	0,871
hyp shHIF-1α	Capn1	1,058	0,000	0,401
	Capza2	1,049	0,855	1,665
	Calm3	1,141	0,985	1,560
	Psma3	0,968	1,079	0,000
hyp scr.vir.co	Pdia3	0,916	0,732	1,113
	Anxa2	1,088	1,367	0,917
	Ldha	0,915	2,765	1,003
hyp scr.vir.co hyp shHIF-1α	Hspa1a	1,010	0,454	0,489
	Ywhaq	1,042	0,610	0,371
	Atp5f1a	1,115	0,714	0,429
	Hsp90ab1	1,175	0,776	0,677
	Pgam1	0,998	1,297	0,560
	Ppp1r12a	0,974	1,490	1,686
	Pgk1	0,835	1,880	0,497
	Hspa5	1,192	2,042	1,631
	Tpi1	0,897	2,081	0,708
	Eno1	1,027	2,142	1,558
	Pkm	1,104	2,982	1,368
norm shHIF-1α hyp shHIF-1α	Nme2	1,259	0,872	0,575
	Rack1	1,836	0,961	0,508
norm shHIF-1α hyp scr.vir.co	Alox12b	2,445	0,445	0,820
	Atp1b1	1,630	0,708	0,822
	Hspb1	1,573	1,245	1,089
	Ap2a2	2,295	1,307	1,195
	Anxa1	2,156	1,343	1,195
	Hspd1	1,519	1,497	0,796
	Prdx2	1,825	1,591	0,878
	Prdx1	2,269	1,860	0,822
	Hsp90aa1	1,237	2,917	0,936
	Arhgef25	4,370	4,739	0,952
norm shHIF-1α hyp scr.vir.co hyp shHIF-1α	Ywhag	1,438	0,177	0,000
	Calr	1,203	0,362	0,360
	Atp1b3	1,583	0,590	0,734
	Rab1A	2,215	0,656	0,710
	S100a4	2,834	1,201	1,702
	Tagln	1,717	1,318	1,392
	Prdx6	2,075	1,349	2,029
	P4hb	1,538	1,436	1,273
	Gapdh	1,330	2,019	1,407
	Pdia6	2,421	2,101	0,000
	Hspa9	1,904	2,414	2,268
	Serpinh1	1,536	2,464	1,450
	Erp29	1,810	2,807	0,000
	Sod1	3,028	2,850	3,116
	Slc25a5	1,677	3,262	1,698
	Clic4	1,958	3,688	2,639
	Gstp1	1,757	3,997	2,458
	Slc25a4	1,684	4,487	1,550
	Ldhc	1,884	4,663	0,000
	Uqcrq	2,147	4,979	0,437

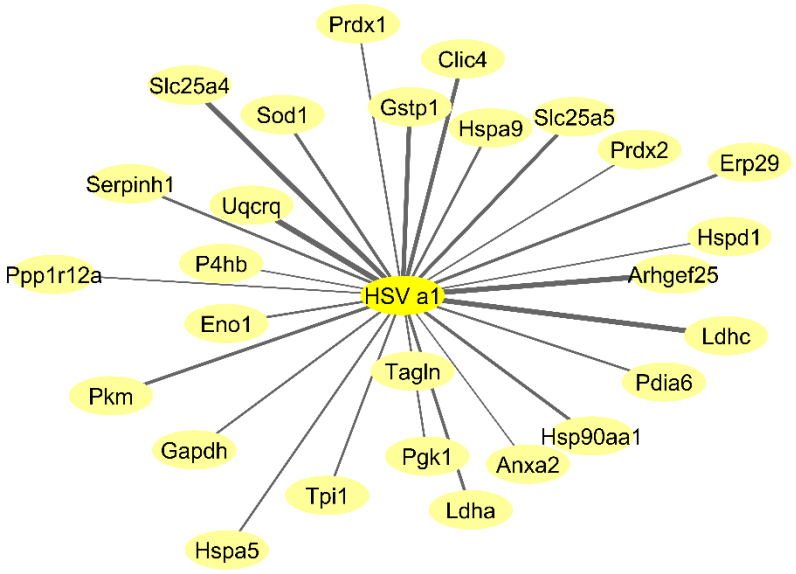

Figure 13: α1 NKA interaction network. α1 NKA interaction network in hypoxic control (scr.vir infected) cells was obtained by using Cytoscape software.

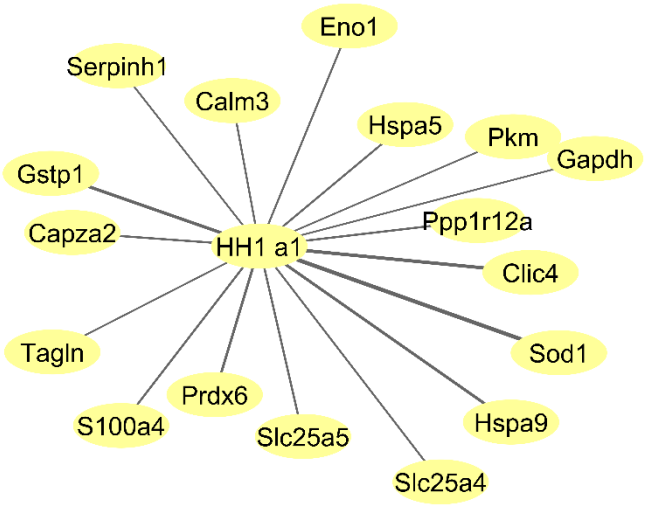

Figure 14: α1 NKA interaction network. α1 NKA interaction network in hypoxic HIF-1α silenced cells was obtained by using Cytoscape software.

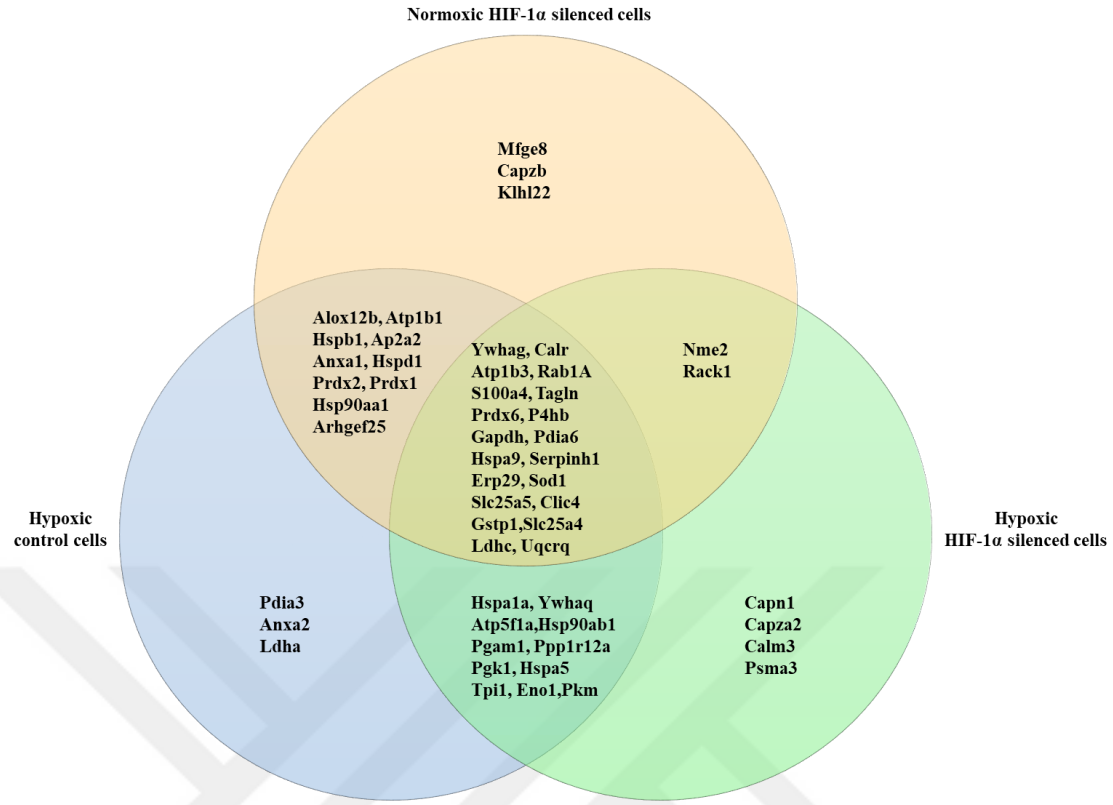

Figure 15: Venn diagram of α1 NKA interacting proteins. The Venn diagram of interacting proteins with α1 NKA in normoxic, hypoxic and HIF-1α silenced cells. Twenty interacting proteins were common in normoxic HIF-1α silenced cells, hypoxic control cells and hypoxic HIF-1α silenced cells.

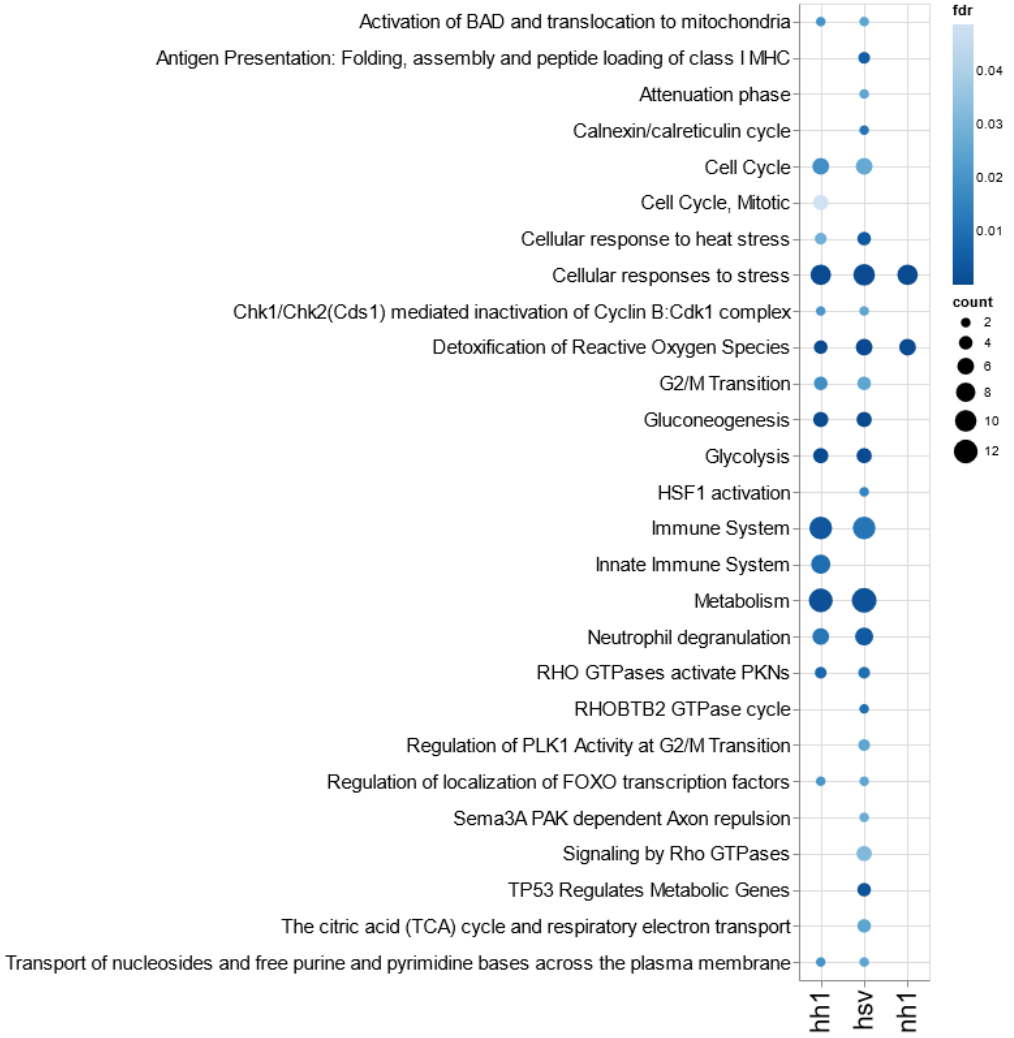

Figure 16: Reactome pathway analysis. Reactome pathway of α1 NKA interactome in normoxic, hypoxic and HIF-1α silenced cells was obtained using STRING DB. nh1: normoxic HIF-1α silenced cells, hsv: hypoxic control cells, hh1: hypoxic HIF-1α silenced cells.

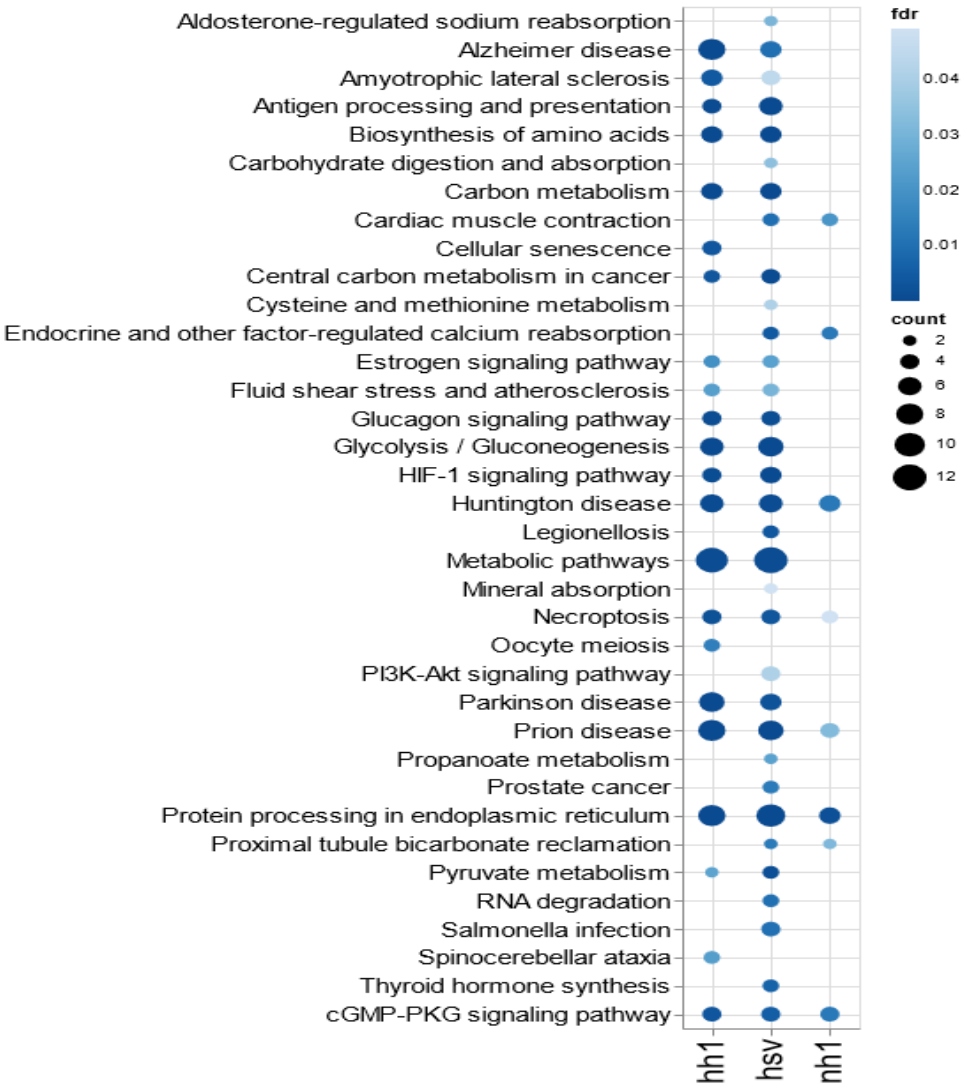

Figure 17: KEGG pathway analysis. KEGG pathway of α1 NKA interactome in normoxic, hypoxic and HIF-1α silenced cells was obtained using STRING DB. nh1: normoxic HIF-1α silenced cells, hsv: hypoxic control cells, hh1: hypoxic HIF-1α silenced cells.

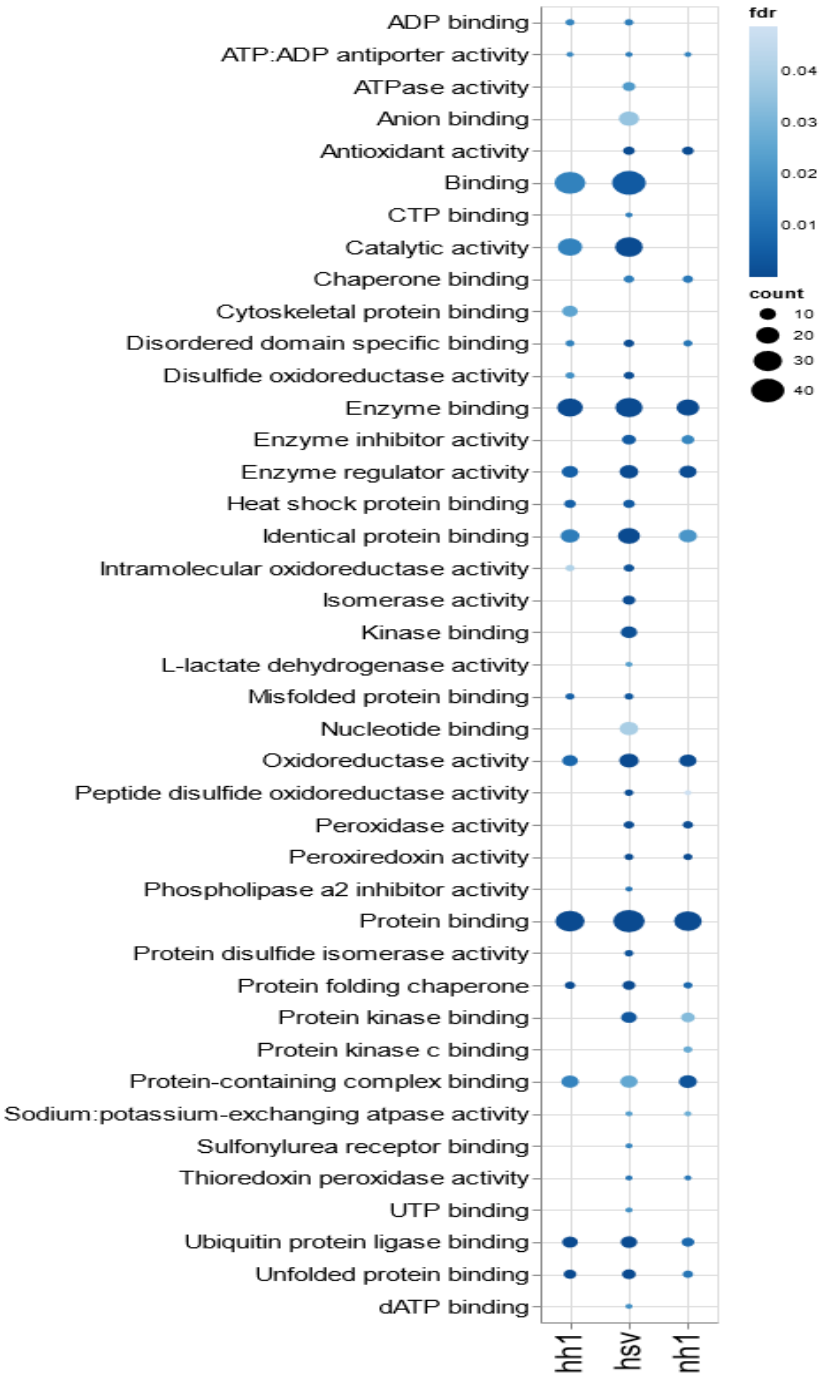

Figure 18: Molecular function analysis. Molecular function of α1 NKA interactome in normoxic, hypoxic and HIF-1α silenced cells was obtained using STRING DB. nh1: normoxic HIF-1α silenced cells, hsv: hypoxic control cells, hh1: hypoxic HIF-1α silenced cells.

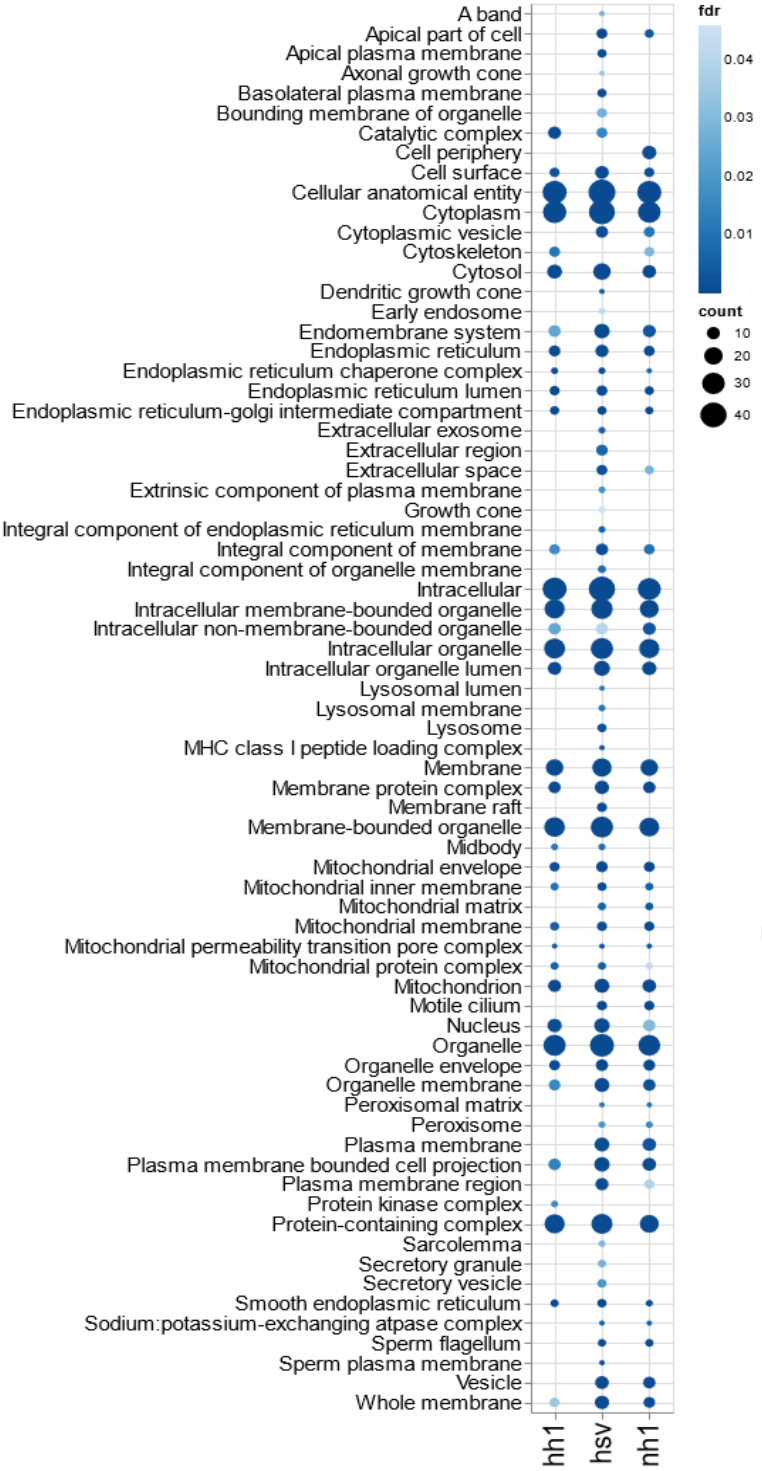

Figure 19: Cellular compartment analysis. Cellular compartment of α1 NKA interactome in normoxic, hypoxic and HIF-1α silenced cells was obtained using STRING DB.
nh1: normoxic HIF-1α silenced cells, hsv: hypoxic control cells, hh1: hypoxic HIF-1α silenced cells.

4.5 Generation of HIF-1α KO H9c2 cells

4.5.1 Annealing of Oligos

Complementary top and bottom oligos were annealed to obtain double stranded guide RNA sequences (sgRNA). The efficiency of annealing was shown by ethidium bromide, which binds to double strand DNA. Figure 20 shows that annealing was successful.

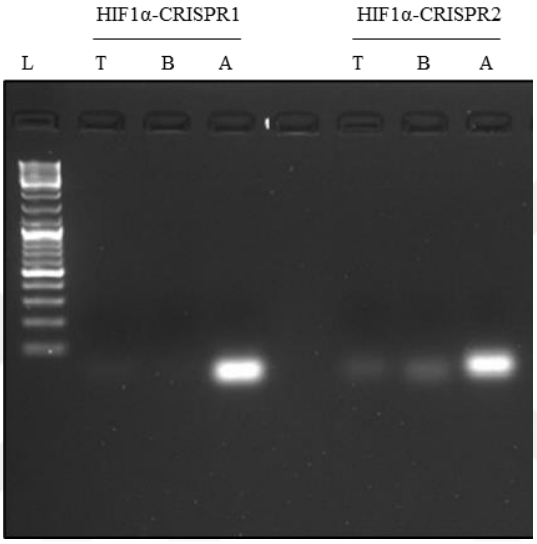

Figure 20: Gel image of annealed oligos. Top, bottom and annealed oligos were run on a 2% agarose gel at 90V for 30 minutes to confirm the success of annealing.

T: Top oligo B: Bottom oligo A: Annealed samples.

4.5.2 Colony PCR

Annealed single guide RNAs (sgRNAs) were cloned into LentiCRISPR v2 plasmid, which were transformed into competent NEB-Stable bacteria. Intact colonies were randomly chosen from the bacterial agar plates for colony PCR. The expected PCR length of the product is 276 bp. No insert and no template were used as control. Figure 21 shows the presence of 276 bp in each colony. Three colonies out of ten were selected and grown in liquid bacterial culture. These colonies were used for miniprep plasmid isolation, and they were sent for Sanger sequencing.

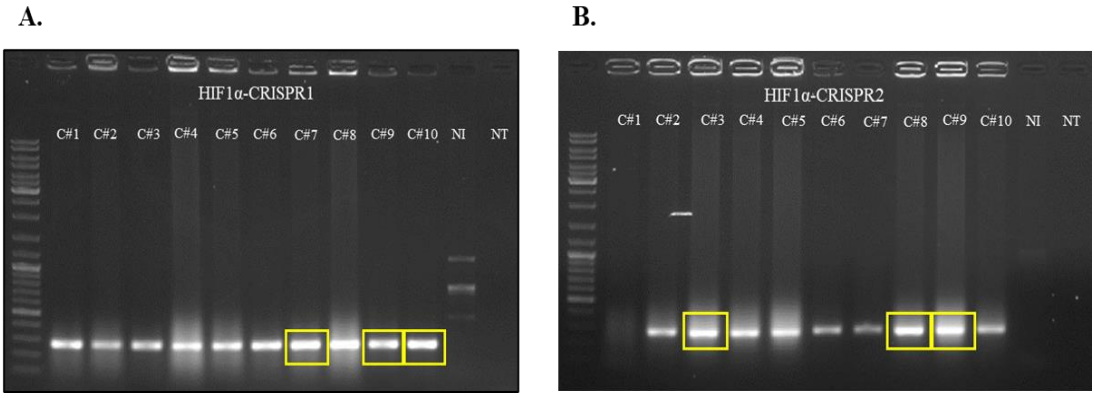

Figure 21: Gel images of selected colonies of sgRNA at the end of colony PCR. Colony 7,9 and 10 were selected for HIF1α-CRISPR1 (A). Colony 3,8 and 9 were selected for HIF1α -CRISPR2 (B). PCR products were run on a 1% agarose gel at 100V for 60 minutes with control groups (no insert and no template groups). Yellow squares indicate the selected colonies for Sanger sequencing. C# (colony number), NI (no insert), NT (no template).

Sanger sequencing results were analysed by using Snap Gene Viewer 5.2.4. Peaks were analysed to check whether there were mismatches, gaps, or insertions. Successful plasmids were selected for next experiments (Figure 22).

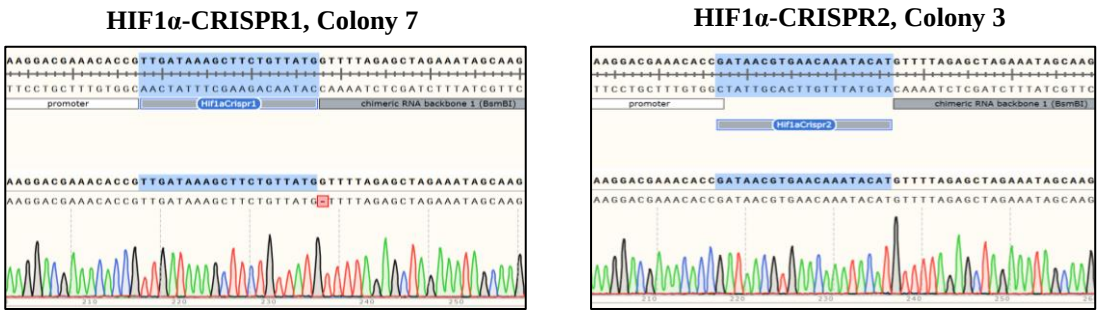

Figure 22: Sanger sequencing analysis of sgRNA. Selected colonies were confirmed by Sanger sequencing. Blue regions indicate the cloned sgRNA sequence in LentiCRISPR v2 plasmid.

4.5.3 Transfection

Restriction enzyme digestion analysis was used to confirm plasmids (Lego G2 Puro, pMDLg-pPRE, pCMV-VSV-g, pRSV-rev) which were digested by using the appropriate restriction enzymes that were shown in Table 21 and predicted fragments were confirmed on agarose gel image (Figure 23).

Table 21: Names of plasmids, suitable restriction enzymes and expected base pair lengths.

Plasmid Name	Enzymes	Expected Fragments Base pair (bp)
Lego G2 Puro	Uncut	8072
Lego G2 Puro	Hind III	556, 590, 998, 1206, 1893, 2829
Lego G2 Puro	Sac I	13, 191, 2390, 2649, 2829
pMDLg-pPRE	Uncut	8890
pMDLg-pPRE	EcoR I	401, 4154, 4335
pMDLg-pPRE	Hind III	627, 897, 3781, 3585
pCMV-VSV-g	Uncut	6507
pCMV-VSV-g	Sac I	691, 5816
pCMV-VSV-g	EcoR I	24, 24, 1668, 4791
pRSV-rev	Uncut	4180
pRSV-rev	EcoR I	311, 3869
pRSV-rev	Hind III	91, 4089

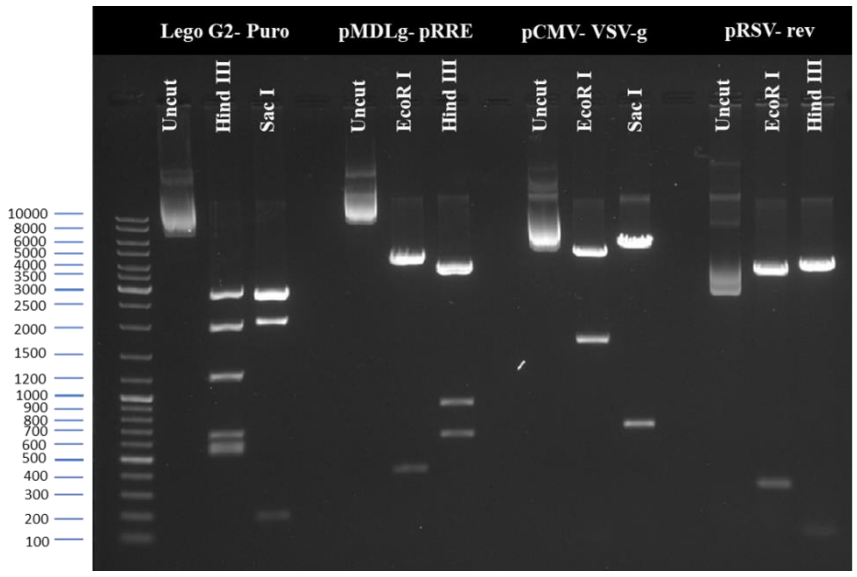

Figure 23: Agarose gel image of the Lego G2-Puro, pMDLg-pPRE, pCMV-VSV-g and pRSV-rev plasmids cut with appropriate enzymes. Samples were run on 1% agarose gel at 100V for 90 minutes.

Eventually, HEK293FT cells were transfected with appropriate plasmids and pcDNA-GFP plasmid carrying GFP marker was used as transfection control to detect whether transfection was efficient or not.

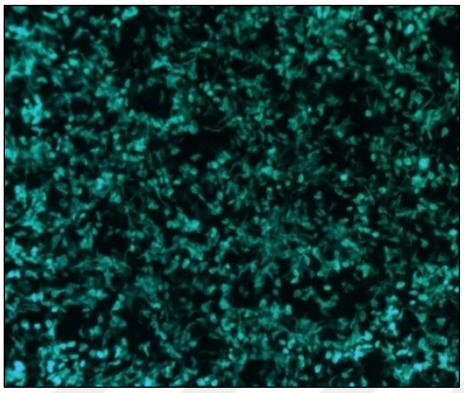

Figure 24: Image of transfection efficiency of HEK293FT cells. Forty eight hours after transfection image was taken under inverted microscope with FITC filter at 10X magnification.

4.5.4 Optimization of PCR Conditions

Gradient PCR was performed at different temperatures using My-Taq DNA polymerase to determine the appropriate required temperature settings for the designed primers. The expected band lengths of the products are shown in Table 22.

Table 22: Names of primers and expected sequence length values.

Primers	**Expected Sequence Length (bp)**
HIF1α-Crispr1	367 bp
HIF1α-Crispr2	334 bp
HIF1α-Crispr1fwd HIF1α-Crispr2rev	1665 bp

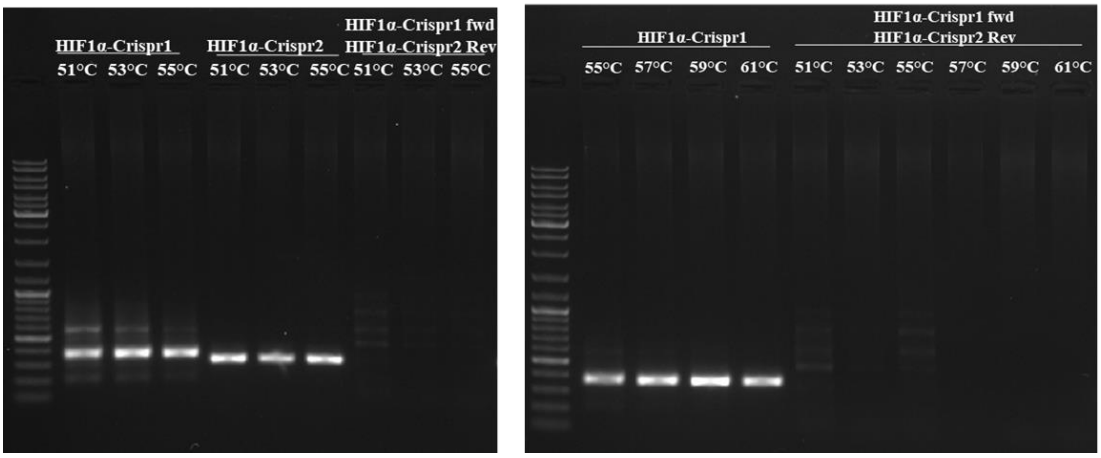

Figure 25: Optimization of temperature for primers. Temperature optimization was performed for each primer.

The optimal temperature for HIF1α-Crispr1fwd-HIF1α-Crispr2rev could not be determined by using My-Taq DNA polymerase so 5X Phusion polymerase with GC buffer was used for HIF1α-Crispr1fwd-HIF1α-Crispr2rev optimization. Different temperatures and different extension time conditions were tested but too many bands were observed so that optimum temperature was not detected. In addition, 5X Phusion polymerase HF buffer was used for HIF1α-Crispr1fwd-HIF1α-Crispr2rev optimization and different temperatures, and primer concentrations were tested. However, appropriate primer temperature could not be optimized even after these experiments.

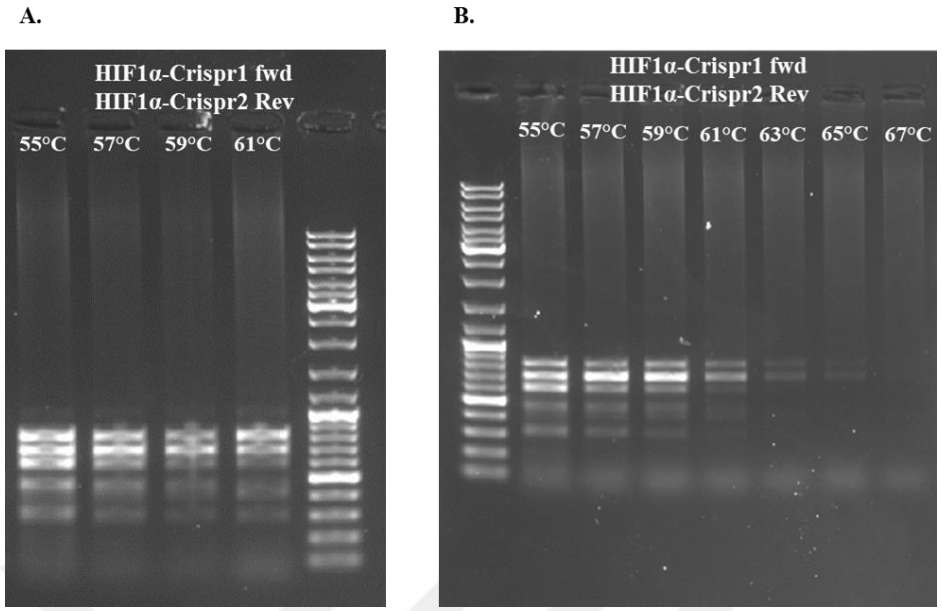

Figure 26: Optimization of temperature for HIF1α-Crispr1fwd- HIF1α-Crispr2rev with 5X Phusion GC buffer. PCR was performed at 4 different temperatures with an extension time of 30 sec.(A). Extension time was set to 60 sec and 7 different temperatures were tested (B).

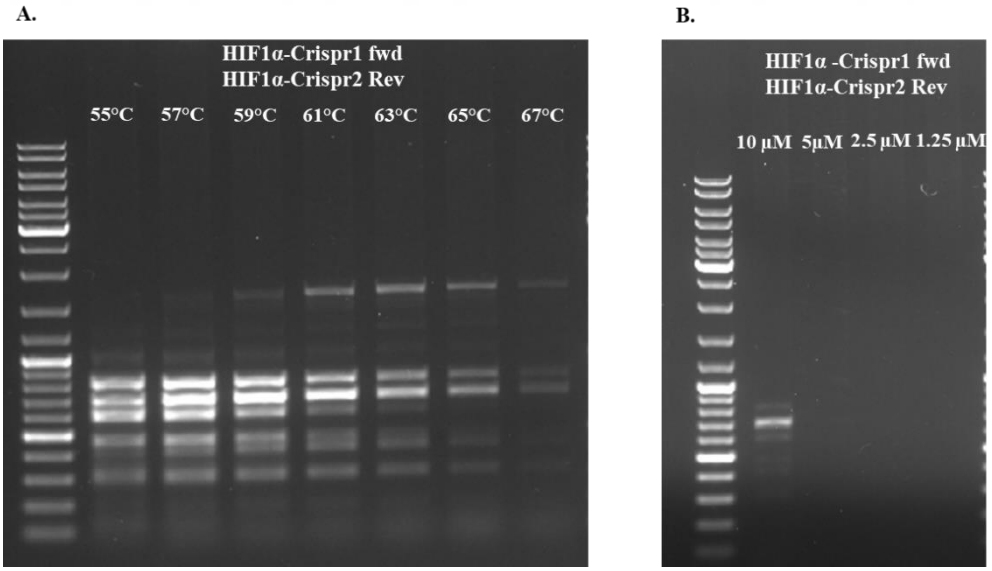

Figure 27: Optimization of temperature for HIF1α-Crispr1fwd- HIF1α-Crispr2rev with 5X Phusion HF buffer. Extension time was set to 60 sec and 7 different temperatures were used (A). Extension time was 60 sec, at 63°C and 4 different primer concentrations were used (B).

4.5.5 Lentiviral Infection

Lentiviruses carry the Puromycin resistance gene, which allows selecting successful infection. To determine the cytotoxic concentration of Puromycin in H9c2 cells, dose-response curves of puromycin were obtained after treating the cells for 24h, 48h and 72h. MTT assay was performed to measure cell viability after indicated times. The IC50 value was calculated according to Puromycin dose-response curves. The concentration of Puromycin to be used in lentiviral infection was determined as 0,4 µg/ml calculated as IC90 value based on 48h of Puromycin. After 2 days, to increase the probability of selection, Puromycin concentration was increased to 1 µg/ml.

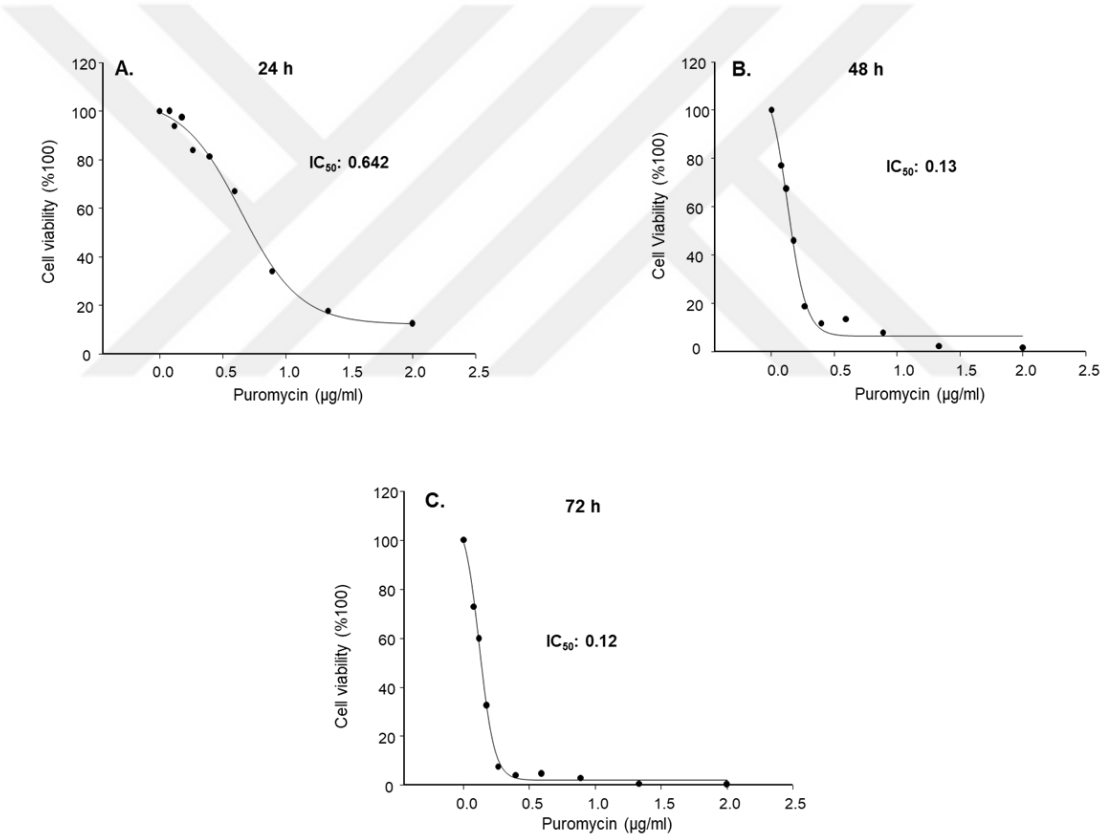

Figure 28: Dose-response curves of Puromycin treatment to check cell viability. H9c2 cells were seeded in 96 well plates and different concentrations of Puromycin was added to the cells for 24 hours (A), 48 hours (B) and 72 hours (C). Cell viability was measured with MTT assay and IC50 values were calculated.

Lentiviruses produced in HEK293FT cells were collected and given to H9c2 cells with Lego G2 puro lentivirus expressing GFP and puromycin resistance gene to check infection efficiency until all cells expressed GFP. It took approximately 27 days for all cells to express GFP in this experimental setup (Figure 29).

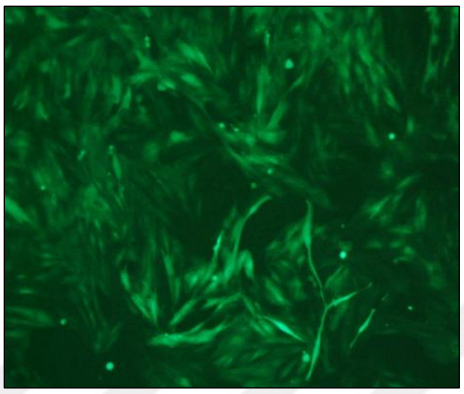

Figure 29: Image of H9c2 cells during Puromycin treatment after GFP expressing Lego G2 puro infection. FITC filter image of cells after 27 days for selection at 10X magnification under inverted microscope.

4.5.6 T7E1 Assay

CRISPR/Cas9 mediated gene editing create breakage in the target genomic DNA by Cas9 and these breaks are repaired by the non-homologous end joining (NHEJ) (60). In NHEJ repair mechanism, nucleotide insertion or deletion may occur and create structural abnormalities in heterogeneous cell population. T7 endonuclease 1 (T7E1) is an enzyme that detects structure abnormalities at target site of DNA. Therefore, target site amplified by on target PCR and PCR products were treated with T7E1 enzyme to calculate the genetic modification in the cell populations. Non-target cells used as control group. According to cut and uncut band intensity, genetic modification rate was calculated. Table 23 shows that genomic modification rate of H1C2 was higher than H1C1. We observed same genomic modification success with H1C1 and H1C2 in other experiments.

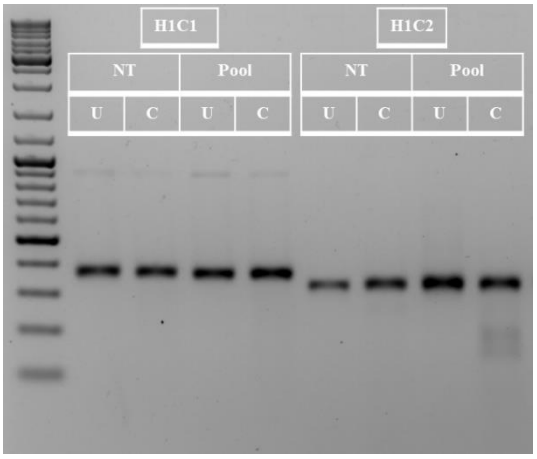

Figure 30: Agarose gel image of PCR products treated and untreated with T7 enzyme. PCR products were run on a 2% agarose gel at 80V for 90 minutes with control group. H1C1: HIF-1α-CRISPR1, H1C2: HIF-1α-CRISPR2, NT: non-target wild type cells. Pool: cell population that infected with lentivirus. U: T7 untreated sample. C: T7 treated sample.

Table 23: The genetic modification rate was calculated according to the band intensity of agarose gel image.

	Non-cleaved Band Intensity	**Cleaved Band Intensity**	**2.Cleaved Band Intensity**	**Fraction**	**%Modification Rate**
H1C1	24,022	0	0	0	0
H1C2	19,795	2,851	0	0,125	6,50

4.6 Protein Expression of HIF-1α in HIF-1α Knockout Cells with CRISPR/Cas9 Gene Editing

To check the efficiency of genomic modifications on the protein level, we measured HIF-1α protein expression. Since HIF-1α is activated under hypoxic conditions, we prepared cell lysates from normoxia or hypoxia (1% O_2, 24h) exposed cells. Figure 31 shows that HIF-1α protein expression was not observed in hypoxic HIF-1α KO cells confirming that genomic modification was successful.

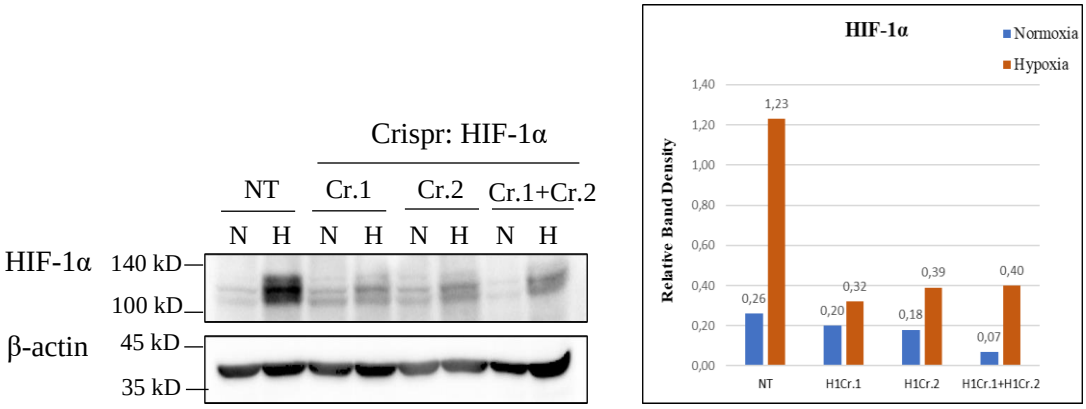

Figure 31: Protein expression of HIF-1α in knockout H9c2 cells. Representative blot of at least three independent experiments. Non target cells were used as control. NT: Non target wild type cells, H1-Cr.1: HIF-1α-CRISPR1, H1-Cr.2: HIF-1α-CRISPR2, H1-Cr1+Cr2: HIF-1α-CRISPR1+CRISPR2. Band densities were measured and normalized to β-actin as loading control. Blue bars represent band density of normoxic cells while orange bars represent band density of hypoxic cells.

HIF-1α gene knockout cells were frozen and kept at -80°C until further use. To test if the cells still maintain their genomic modification after freeze thawing, we cultured them again in Puromycin containing medium. The protein expression of HIF-1α was examined, and the efficiency of HIF-1α KO was found to be low when cells were reopened and grown again (Figure 32).

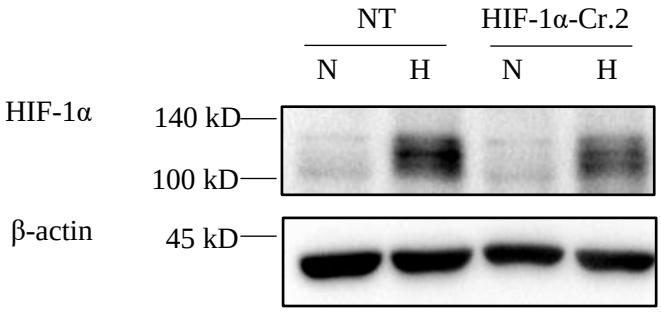

Figure 32: HIF-1α expression in knockout cells after re-culture. Non target cells used as a control. β-actin was used as loading control. NT: Non-target, HIF-1α-Cr.2: HIF-1α-CRISPR2.

Based on the result above, we thought cells may be losing their genotypic changes due to recovery after thawing and culturing. We re-infected these re-cultured cells with lentiviruses and selected with Puromycin to examine if a second infection would increase the success rate. HIF-1α expression was measured by Western Blot. Figure 33 shows that a second lentiviral infection successfully deleted HIF-1α.

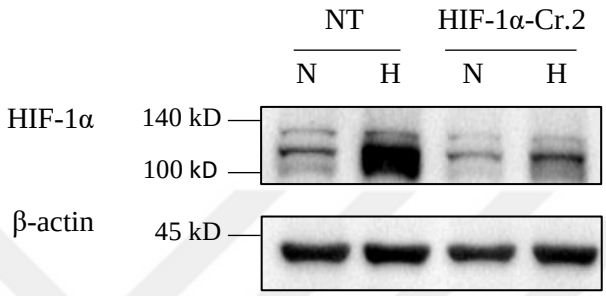

Figure 33: Protein expression of HIF-1α from knockout cells that were re-infected with the same amount of lentiviruses used previously. Non target cells used as control. β-actin was used as loading control. NT: Non-target, HIF-1α-Cr.2: HIF-1α-CRISPR2.

We also checked the expression of α1 NKA from one of the frozen HIF-1α KO cells whether results obtained from shHIF-1α infected cells would also be observed in HIF-1α KO cells as well. We performed cell membrane biotinylation assay and measured membrane and intracellular expression of α1 NKA from normoxic and hypoxic HIF-1α KO cells.

Figure 34 shows at the plasma membrane no hypoxic inhibition occurs in control cells and HIF-1α-CRISPR2 does not have any effect on the membrane expression of α1 NKA. This result indicated that frozen, re-cultured and re-infected cells may be already under stress and may have adapted to hypoxic stress. Therefore, we concluded that re-cultured and re-infected cells may not be suitable for these experiments.

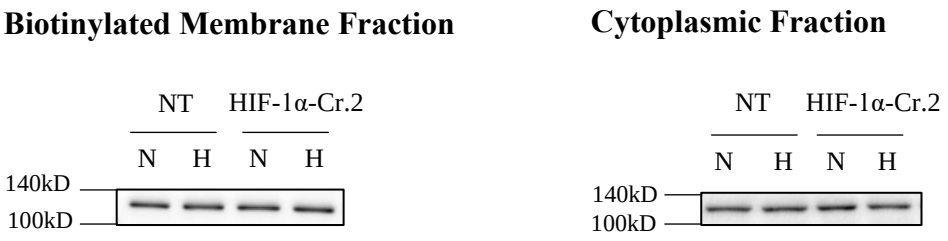

Figure 34: Expression of α1 NKA subunit in membrane and cytoplasmic fraction from HIF-1α KO cells that were frozen, re-cultured and infected again. NT: Non-target, HIF-1α-Cr.2: HIF-1α-CRISPR2.

4.7 Generation of HIF-1α KO Single Cell Colonies

HIF-1α knockout single cell colonies, were selected and grown under Puromycin selection as described in methods section. Selected colonies were grown to confluency and frozen for future studies. Nine colonies were screened sequentially. To examine whether the HIF-1α gene is deleted in the colonies grown from single cells, targeted region in HIF-1α genome was amplified using primers designed from outside the cut regions of the CRISPR sgRNAs. If two CRISPR worked together in two alleles, it would be expected that a shorter band or no band would be seen compared to non-target, since the region in between would be deleted. Screening single cell colonies showed that the designed one or two CRISPR did not work (Figure 35).

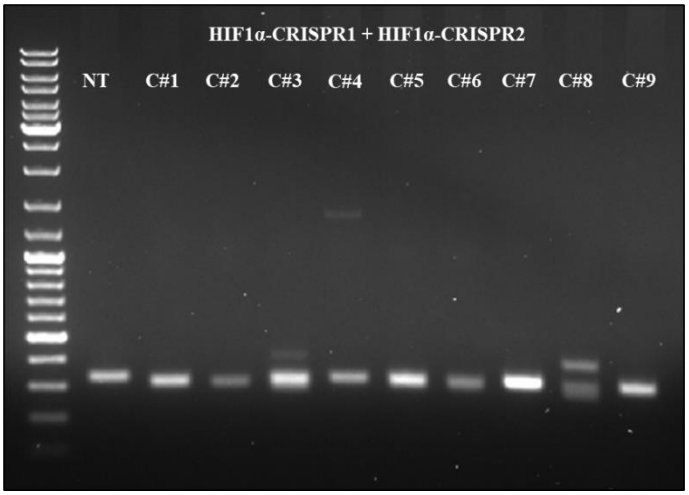

Figure 35: Agarose gel image of PCR product of single cell colonies. PCR products were run on 1% agarose gel at 100V for 60 minutes with control. C# (colony number), NT (Non-target).

5. DISCUSSION AND CONCLUSION

The activity of the $Na^{+/}K^{+}$-ATPase (NKA) pump is critical for the optimal function of the heart. NKA activity is impaired in cardiac ischemia and heart failure. This results in detrimental effects on the heart such as Ca^{2+} overload, diastolic dysfunction, and development of arrythmias (35). Studies reported that decreased activity of the NKA pump is due to decreased protein expression of the α1, α3 and β1 subunits (37). About ~30% reduction in the pump activity was observed in tissue homogenates obtained from different animal species used in in-vivo heart failure models, while 40% reduction was observed in human necropsy materials with heart failure (35). However, it is not known how the expression of NKA is regulated in the ischemic heart, which signalling pathways participate in this process and whether increased HIF-1α activity in cardiac ischemia has a role in this regulation.

This thesis study focused on this question by investigating the regulation of α1 NKA, the catalytic subunit of NKA, in H9c2 cardiomyocytes using in-vitro hypoxia as an ischemic heart model and comprehensively identified regulatory signalling pathways. Here the presented study showed first time that plasma membrane expression of α1 NKA, decreased in hypoxia due to internalization and degradation. Silencing HIF-1α gene expression prevented the degradation of α1 NKA in hypoxic cells. Using immunoprecipitation (IP) based proteomic and bioinformatic analysis we also identified that in hypoxia α1 NKA interacted with molecular chaperones which regulate the quality control processes of the newly synthesized proteins in endoplasmic reticulum (ER), and specifically interact with α1 NKA in HIF-1α sensitive manner.

In studies investigating the expression of the pump subunits in ischemic heart and heart failure models, measurements have been performed from tissue homogenates or total cell lysates from the isolated cells. Based on these studies, Semb et al., 1998 showed that there was no significant change in protein and mRNA expressions of α1 NKA in the control and congestive heart failure (CHF) groups (36). However, Schwinger et al., 1999 found that α1 NKA protein expression was significantly reduced in failing myocardium compared to the non-failing left ventricular myocardium (37). According to Allen et al., 1992, α1 NKA was expressed in human

heart and there was no change in α1 NKA mRNA expression between the normal heart and heart failure (61). However, Shamraj et al.,1993 found that the mRNA expression of α1 NKA was different in failing human hearts. Protein level of α1 NKA was lower in failing heart than the non-failing heart (62,63). In our previous studies, we showed that mRNA expression of α1 NKA was reduced approximately 10% in hypoxic cells (data was not shown). Therefore, literature report inconsistent findings about the expression of α1 NKA in the ischemic heart. Most of these experiments in these studies have been performed with total homogenates of the tissues which do not purely reflect the expression of the proteins at plasma membrane compartment where the active pump molecules are located; rather, they represent the total expression of proteins, since these materials include other compartments in the cells such as the cytoplasm and lysosome. Therefore, the relative changes in the membrane and intracellular expression of the α1 NKA needed to be investigated detailly in cell compartments.

In the presented study here, the expression of α1 NKA was investigated at the plasma membrane and intracellular compartment of the cells using Sulfo-NHS-SS-Biotin which does not penetrate the cells, and which reacts with primary amino groups (-NH2) of the proteins located at the cell surface. Biotinylated proteins were pulled down with Streptavidin resins that specifically bind to biotin. Therefore, separated biotin-bound and unbound fractions from total cell lysates represent plasma membrane and intracellular fractions of the cells, which were then investigated by SDS-PAGE and Western Blot. According to the data, membrane expression of the α1 NKA decreased by hypoxia while, its internalization and degradation increased. Silencing HIF-1α gene expression abolished the degradation of the α1 NKA in hypoxic cells. Also, membrane expression of α1 NKA increased in hypoxic HIF-1α silenced cells compared to the hypoxic control cells. Therefore, silencing of HIF-1α by preventing the degradation increased the translocation of α1 NKA to the membrane. Our results demonstrated for the first time that increased HIF-1α activity, which is common in ischemic heart diseases participate in regulating α1 NKA in hypoxic cells.

To further understand the detailed mechanism of α1 NKA regulation in hypoxic and HIF-1α silenced cells, we performed comparative and comprehensive analysis of interacting protein partners of α1 NKA after performing IP and proteomic studies. Overall, the interactome analysis showed that α1 NKA interacting partners are mostly

located at the mitochondria, protein containing complexes, membrane bounded organelles, intracellular compartment, endoplasmic reticulum, and cytoplasm.

Reactome pathway analysis showed that, cellular responses to stress such as Calnexin/calreticulin cycle and HSF-1 pathway increased with hypoxia and disappeared in HIF-1α silenced hypoxic cells.

KEGG pathway analysis provide high-level functions and utilities of the biological systems (64). Our analysis demonstrated that HIF-1α signalling, glycolysis/gluconeogenesis, PI3K-Akt and metabolic pathways increased with hypoxia and decreased in hypoxic HIF-1α silenced cells. Proteins involved in cardiac muscle contraction increased in hypoxic control cells compared to normoxic HIF-1α silenced cells and it disappeared in hypoxic HIF-1α silenced cells. These data showed that, hypoxia induced different cellular stress pathways in cardiomyocytes, which have divergent roles in signalling, survival, and metabolism.

Molecular function analysis revealed that ubiquitin protein ligase binding increased with hypoxia and slightly decreased in normoxic HIF-1α silenced cells. In addition, unfolded protein binding increased with hypoxia and no change was observed with silencing HIF-1α. Protein kinase binding has important role in different signalling mechanism, and it increased in hypoxic control cells (65).

In α1 NKA interactome 53 unique interaction partners were identified (Table 20). In literature β1 NKA has been reported to regulate the membrane insertion and expression of α1 NKA (21). In our study we also identified β1 NKA as interacting partner of α1 NKA, thus confirmed literature report. The interaction of β3 with α1 NKA is shown for the first time in our study. Comparative analysis showed that β1 and β3 NKA abundance ratio decreased in hypoxic cells compared to normoxic cells; and HIF-1α silencing slightly increased their interaction. Whether these altered interactions affect the membrane insertion of α1 NKA and the activity of the pump needs to be clarified in future experiments.

Our study also identified proteins that play role in cell metabolism and glycolysis such as GAPDH, LDH, PKM, ENO1. Their abundance ratios increased with hypoxia and silencing HIF-1α abolished the interactions.

Moreover, the cytosolic chaperones heat shock protein Hsp1,5, Erp29, Hsp90aa1, Hsp47 and protein disulfide isomerase (PDI) related with endoplasmic reticulum (ER)

homeostasis (66) have increased abundance ratio in hypoxia and they were sensitive to HIF-1α silencing. Among these interaction partners Hsp47 function as a chaperone in collagen biosynthesis pathway and controls proper protein folding for quality control in the ER (67).

Under stress conditions such as lack of nutrients and oxygen, maturation of the proteins and their proper folding in the ER is impaired. Therefore, cells have developed unfolded protein response (UPR) to fight against ER stress and it is activated in response to misfolded or unfolded proteins resident in ER (68). UPR system consist of different signaling branches and inositol-requiring enzyme 1 (IRE1) is one of the key proteins in the ER (58). In the absence of any cellular stress, Hsp47 binds to the luminal domain of IRE1 for the oligomerization of IRE1 (58). Hypoxic stress triggers cascade of events and leads to activation of ubiquitin proteasome pathway (UPP) system (69,70). In cellular stress Hsp47 disassociates from IRE1 and binds to unmatured/unfolded/misfolded proteins to prevent their transport into Golgi for further cellular processes (71).

Our analysis showed that hypoxia increased α1 NKA-Hsp47 abundance ratio by 2.5-fold, and this interaction decreased to normoxic ratio in HIF-1α silenced hypoxic cells. Therefore, hypoxia might have induced UPR and that may have caused α1 NKA retention in the ER and prevented further processing. This process seems sensitive to HIF-1α silencing (72). The interaction of α1 NKA with Hsp47 and its relationship with the UPR system has not been reported in the literature before. This relationship has been demonstrated for the first time in our studies. Whether this interaction is due to increased Hsp47 expression or activity in hypoxic cells needs further clarification.

Also, we identified Hsp90aa1 as an interacting partner of α1 NKA in hypoxic cells. Hsp90aa1 is the inducible form of Hsp90 (73) which is a well conserved chaperone protein for the cells to survive under stress (74). Abundance ratio of Hsp90aa1, increased by 3 fold in hypoxic cells and this interaction decreased to normoxic ratio in HIF-1α silenced cells. Again, whether this interaction is due to increased expression of Hsp90aa1 in hypoxic cells needs to be addressed in future studies.

Hsp70 has been implicated in restoring of the cytoskeletal anchoring of NKA. According to Riordan et al., 2005, NKA plays critical role in osmoregulation in

mammalian kidney. In renal damage, Hsp70 was linked to NKA in pig kidney epithelial cell line LLC-PK1 (75). Ruete et al., 2008 showed that Hsp70 and NKA interaction was increased in rats after their recovery from low protein diet (76). All these studies demonstrated that under stress condition like nutritional stress, Hsp70 was activated for maintaining the function of NKA (77). In our analysis, the interaction of α1 NKA with Hspa1a, Hspa5, Hspa9 (members of heat shock protein 70 family) has been also identified. For example, Hspa1a-α1 NKA abundance ratio decreased in hypoxic cells. Abundance ratio of Hspa5-α1 NKA increased in hypoxia, and it was partially sensitive to HIF-1α silencing. Hspa9-α1 NKA abundance ratio only increased in hypoxic cells. These results suggest different interactions profiles of Hsp70 family proteins with α1 NKA in cardiomyocytes, which needs clarification.

Coppi and Guidotti 1997 were first suggested ubiquitination of the NKA in 1997. They reported that α1 and α2 subunits of NKA can be regulated via polyubiquitination in COS-7 cells (78). In addition, Helenius, Dada and Sznajder., 2010 showed that exposure of alveolar epithelial cells to the hypoxia generate reactive oxygen species which activated PKC-ζ for phosphorylation of NKA and proposed ubiquitination-endocytosis-degradation mechanism (79). However, in ischemic heart an UPR and ER stress dependent regulation of NKA has been first time shown in this study.

Taken together, proteomic analysis revealed new protein interacting partners of α1 NKA in cardiomyocytes under normoxic and hypoxic conditions that have not been previously reported in the literature with some of them being HIF-1α sensitive. For example, Hsp47, Hsp90aa1, β3 NKA, Erp29, Eno1, Scl25a5, Scl25a4, Uqcrq, Clic4.

Based on these findings, we propose that protein synthesis and degradation processes are different in normoxic and hypoxic conditions. In normoxia when there is no cellular stress, while some proteins are degraded, most of them are retrieved from recycling pool and transferred to the membrane or cellular compartment. On the other hand, UPR system, ER stress and the ubiquitin proteosome pathway are activated in hypoxia and α1 NKA might be retained in the ER or degraded, causing decreased insertion to plasma membrane. Silencing HIF-1α reversed this process and protected α1 NKA from degradation and increased the insertion of the protein to plasma membrane. The process of α1 NKA in UPP and UPR system and the activity of NKA needs to be detailly studied in future studies.

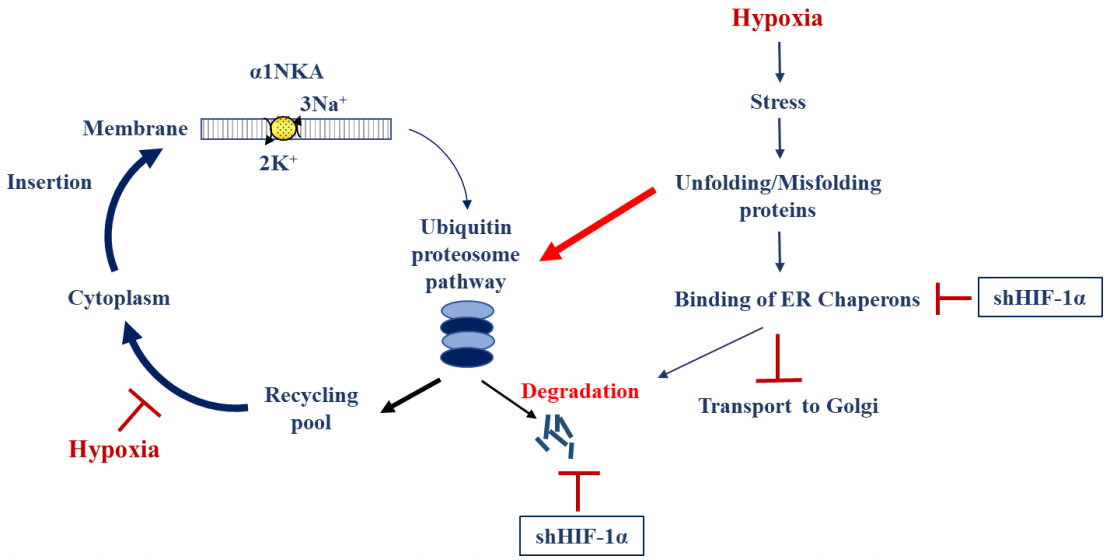

Figure 36: Summary. Regulation process of α1 NKA in normoxic (A) and hypoxic cardiomyocytes (B). Hypoxia activates ER stress and cause degradation of the α1-NKA.

Another aim of this study was to generate HIF-1α knockout H9c2 cell line as a model to study the role of HIF-1α in in-vitro ischemic heart studies. For this purpose, we used the most effective gene editing system, CRISPR/Cas9 lentiviral system. In CRISPR/Cas9 gene editing, Cas9 enzyme cuts the target region, and this region is repaired by DNA repair mechanisms. During the DNA repair, nucleotide insertion or deletion may occur, and it may cause frameshift mutations (80). Consequently, each cell in the cell pool receives random genome editing. Therefore, T7E1 assay was performed to detect genetic modification rate in HIF-1α deleted cell pools. We observed that modification rate of H1C2 was more successful than H1C1. Protein levels of HIF-1α in CRISPR/Cas9 modified cells and non-target control cells were measured by Western Blot. HIF-1α KO efficiency was found ~80% at the protein level and considered successful and HIF-1α KO H9c2 cell line was frozen for further use.

Before measuring the expression of α1 NKA to determine if the cells still maintain their genomic modification after freeze and thawing, HIF-1α expression was measured in normoxic and hypoxic cells. Efficiency of HIF-1α KO was found to be low (~30%) and it was thought that HIF-1α KO cells might recovered after freezing and thawing.

This may be explained by that in some cells CRISPR/Cas9 gene editing is not always persistently successful (60). There may be several reasons for this observation: (1) some cells did not take up the plasmid and they overgrew while KO cells were recovering, (2) some cells successfully import the plasmid into the cell, but depending on proliferation or maturation status of the cell defence mechanisms against stress might have overcome genome modification, (4) cells take the plasmid but genome editing can be successful for only in one of the two alleles, in the cells that may have multi nuclei in their nature as in cardiomyocytes (60).

In addition, membrane, and intracellular expression of α1 NKA in KO cells kept in hypoxia and infected with shHIF-1α adenovirus differs from cells infected with lentiviruses. Hypoxia exposure of control CRISPR/Cas9 infected cells did not have decreased expression of α1 NKA. We concluded that frozen, re-cultured and re-infected cells may be under more stress condition and cells may have adapted to hypoxic stress.

Therefore, it was important to separate cells in the heterozygous cell pool and find homozygous cells where deletion of HIF-1α gene occurs in two alleles. To obtain HIF-1α homozygous cell, we generated HIF-1α KO single cell colonies and screened them. However, the cells grown from single cell colonies were not homozygous for HIF-1α KO. In addition, HIF-1α-CRISPR1 primer could not be optimized so that the genetic modification rates of these cells could not be calculated and interpreted.

In conclusion, this Master's thesis study identified new protein interacting partners of α1 NKA and that ER stress dependent signalling might control its regulation in the ischemic heart, which seems to be dependent of HIF-1α. The mechanisms by which these identified proteins interact and regulate the expression and thus the activity of NKA in ischemic heart needs to be investigated in future studies. This study provided new information about regulation of NKA in the ischemic heart and defined a signalling mechanism behind that.

6.REFERENCES

1. Cardiovascular diseases (CVDs). [2022 Jul 30]. Available from: https://www.who.int/en/news-room/fact-sheets/detail/cardiovascular-diseases-(cvds)

2. Cardiovascular diseases. [2022 Jul 30]. Available from: https://www.who.int/health-topics/cardiovascular-diseases/#tab=tab_3

3. Cardiovascular disease: heart disease causes and symptoms. [2022 Jul 30]. Available from: https://my.clevelandclinic.org/health/diseases/21493-cardiovascular-disease

4. Semenza GL. Oxygen sensing, hypoxia-inducible factors, and disease pathophysiology. Annu Rev Pathol. 2014;9:47-71.

5. Ren JL, Chen Y, Zhang LS, Zhang YR, Liu SM, Yu YR, Jia MZ, Tang CS, Qi YF, Lu WW. Intermedin1-53 attenuates atherosclerotic plaque vulnerability by inhibiting CHOP-mediated apoptosis and inflammasome in macrophages. Cell Death Dis. 2021 May 1;12(5):436.

6. Liu M, Galli G, Wang Y, Fan Q, Wang Z, Wang X, Xiao W. Novel Therapeutic Targets for Hypoxia-Related Cardiovascular Diseases: The Role of HIF-1. Front Physiol. 2020 Jul 15;11:774.

7. Semenza GL. Hypoxia-inducible factor 1 and cardiovascular disease. Annu Rev Physiol. 2014;76:39-56.

8. Hwang KC, Lim S, Kwon HM, Bae YS, Kang SM, Chung KH, Graham RM, Rhee SG, Jang Y. Phospholipase C-delta1 rescues intracellular Ca2+ overload in ischemic heart and hypoxic neonatal cardiomyocytes. J Steroid Biochem Mol Biol. 2004 Jul;91(3):131-8.

9. Laham RJ, Chronos NA, Pike M, Leimbach ME, Udelson JE, Pearlman JD, Pettigrew RI, Whitehouse MJ, Yoshizawa C, Simons M. Intracoronary basic fibroblast growth factor (FGF-2) in patients with severe ischemic heart disease: results of a phase I open-label dose escalation study. J Am Coll Cardiol. 2000 Dec;36(7):2132-9.

10. Iravanian S, Dudley SC Jr. The renin-angiotensin-aldosterone system (RAAS) and cardiac arrhythmias. Heart Rhythm. 2008 Jun;5(6 Suppl):S12-7.

11. Stanley WC. Changes in cardiac metabolism: a critical step from stable angina to ischaemic cardiomyopathy. Eur Heart J. 2001;3(Supply O):S02-07.

12. Agrawal V, Gupta JK, Qureshi SS, Vishwakarma VK. Role of cardiac renin angiotensin system in ischemia reperfusion injury and preconditioning of heart. Indian Heart J. 2016 Nov-Dec;68(6):856-861.

13. Bers DM. Cardiac excitation-contraction coupling. Nature. 2002 Jan 10;415(6868):198-205.

14. Despa S, Bers DM. Na^+ transport in the normal and failing heart - remember the balance. J Mol Cell Cardiol. 2013 Aug;61:2-10.

15. Padrón R, Ma W, Duno-Miranda S, Koubassova N, Lee KH, Pinto A, Alamo L, Bolaños P, Tsaturyan A, Irving T, Craig R. The myosin interacting-heads motif present in live tarantula muscle explains tetanic and posttetanic phosphorylation mechanisms. Proc Natl Acad Sci U S A. 2020 Jun 2;117(22):11865-11874.

16. Bers DM, Despa S. Na+ transport in cardiac myocytes; Implications for excitation-contraction coupling. IUBMB Life. 2009 Mar;61(3):215-21.

17. Brini M, Carafoli E. The plasma membrane Ca^{2+} ATPase and the plasma membrane sodium calcium exchanger cooperate in the regulation of cell calcium. Cold Spring Harb Perspect Biol. 2011 Feb 1;3(2):a004168.

18. Baartscheer A, Schumacher CA, van Borren MM, Belterman CN, Coronel R, Fiolet JW. Increased Na+/H+-exchange activity is the cause of increased [Na+]i and underlies disturbed calcium handling in the rabbit pressure and volume overload heart failure model. Cardiovasc Res. 2003 Mar 15;57(4):1015-24.

19. Bers DM, Barry WH, Despa S. Intracellular Na+ regulation in cardiac myocytes. Cardiovasc Res. 2003 Mar 15;57(4):897-912.

20. Silva CID, Gonçalves-de-Albuquerque CF, Moraes BPT, Garcia DG, Burth P. Na/K-ATPase: Their role in cell adhesion and migration in cancer. Biochimie. 2021 Jun;185:1-8.

21. Wen XP, Wan QQ. Regulatory effect of insulin on the structure, function and metabolism of Na+/K+-ATPase (Review). Exp Ther Med. 2021 Nov;22(5):1243.

22. Yan Y, Shapiro JI. The physiological and clinical importance of sodium potassium ATPase in cardiovascular diseases. Curr Opin Pharmacol. 2016 Apr;27:43-9.

23. Berry RG, Despa S, Fuller W, Bers DM, Shattock MJ. Differential distribution and regulation of mouse cardiac Na+/K+-ATPase alpha1 and alpha2 subunits in T-tubule and surface sarcolemmal membranes. Cardiovasc Res. 2007 Jan 1;73(1):92-100.

24. Morth JP, Pedersen BP, Toustrup-Jensen MS, Sørensen TL, Petersen J, Andersen JP, Vilsen B, Nissen P. Crystal structure of the sodium-potassium pump. Nature. 2007 Dec 13;450(7172):1043-9.

25. Geering K. Functional roles of Na,K-ATPase subunits. Curr Opin Nephrol Hypertens. 2008 Sep;17(5):526-32.

26. Grandi E, Herren AW. CaMKII-dependent regulation of cardiac Na(+) homeostasis. Front Pharmacol. 2014 Mar 10;5:41.

27. Tian J, Cai T, Yuan Z, Wang H, Liu L, Haas M, Maksimova E, Huang XY, Xie ZJ. Binding of Src to Na+/K+-ATPase forms a functional signaling complex. Mol Biol Cell. 2006 Jan;17(1):317-26.

28. McDonough AA, Velotta JB, Schwinger RH, Philipson KD, Farley RA. The cardiac sodium pump: structure and function. Basic Res Cardiol. 2002;97 Suppl 1:I19-24.

29. Yan Y, Shapiro AP, Mopidevi BR, Chaudhry MA, Maxwell K, Haller ST, Drummond CA, Kennedy DJ, Tian J, Malhotra D, Xie ZJ, Shapiro JI, Liu J. Protein Carbonylation of an Amino Acid Residue of the Na/K-ATPase α1 Subunit Determines Na/K-ATPase Signaling and Sodium Transport in Renal Proximal Tubular Cells. J Am Heart Assoc. 2016 Sep 9;5(9):e003675.

30. Bouzinova EV, Hangaard L, Staehr C, Mazur A, Ferreira A, Chibalin AV, Sandow SL, Xie Z, Aalkjaer C, Matchkov VV. The α2 isoform Na,K-ATPase modulates contraction of rat mesenteric small artery via cSrc-dependent Ca2+ sensitization. Acta Physiol (Oxf). 2018 Sep;224(1):e13059.

31. Cui X, Xie Z. Protein Interaction and Na/K-ATPase-Mediated Signal Transduction. Molecules. 2017 Jun 14;22(6):990.

32. Pike MM, Luo CS, Clark MD, Kirk KA, Kitakaze M, Madden MC, Cragoe EJ Jr, Pohost GM. NMR measurements of Na+ and cellular energy in ischemic rat heart: role of Na(+)-H+ exchange. Am J Physiol. 1993 Dec;265(6 Pt 2):H2017-26.

33. Jeremy RW, Ambrosio G, Pike MM, Jacobus WE, Becker LC. The functional recovery of post-ischemic myocardium requires glycolysis during early reperfusion. J Mol Cell Cardiol. 1993 Mar;25(3):261-76.

34. Despa S, Islam MA, Pogwizd SM, Bers DM. Intracellular [Na+] and Na+ pump rate in rat and rabbit ventricular myocytes. J Physiol. 2002 Feb 15;539(Pt 1):133-43.

35. Pogwizd SM, Sipido KR, Verdonck F, Bers DM. Intracellular Na in animal models of hypertrophy and heart failure: contractile function and arrhythmogenesis. Cardiovasc Res. 2003 Mar 15;57(4):887-96.

36. Semb SO, Lunde PK, Holt E, Tønnessen T, Christensen G, Sejersted OM. Reduced myocardial Na+, K(+)-pump capacity in congestive heart failure following myocardial infarction in rats. J Mol Cell Cardiol. 1998 Jul;30(7):1311-28.

37. Schwinger RH, Wang J, Frank K, Müller-Ehmsen J, Brixius K, McDonough AA, Erdmann E. Reduced sodium pump alpha1, alpha3, and beta1-isoform protein levels and Na+,K+-ATPase

activity but unchanged Na+-Ca2+ exchanger protein levels in human heart failure. Circulation. 1999 Apr 27;99(16):2105-12.

38. Kihara Y, Grossman W, Morgan JP. Direct measurement of changes in intracellular calcium transients during hypoxia, ischemia, and reperfusion of the intact mammalian heart. Circ Res. 1989 Oct;65(4):1029-44.

39. Jewell UR, Gassmann M. Mammalian gene expression in hypoxic conditions. Zoology (Jena). 2001;104(3-4):192-7.

40. Liu L, Simon MC. Regulation of transcription and translation by hypoxia. Cancer Biol Ther. 2004 Jun;3(6):492-7.

41. Lucero García Rojas EY, Villanueva C, Bond RA. Hypoxia Inducible Factors as Central Players in the Pathogenesis and Pathophysiology of Cardiovascular Diseases. Front Cardiovasc Med. 2021 Aug 10;8:709509.

42. Semenza GL. Defining the role of hypoxia-inducible factor 1 in cancer biology and therapeutics. Oncogene. 2010 Feb 4;29(5):625-34.

43. Semenza GL. Hypoxia-inducible factors in physiology and medicine. Cell. 2012 Feb 3;148(3):399-408.

44. Guo Y, Xiao Z, Yang L, Gao Y, Zhu Q, Hu L, Huang D, Xu Q. Hypoxia-inducible factors in hepatocellular carcinoma (Review). Oncol Rep. 2020 Jan;43(1):3-15.

45. Berra E, Benizri E, Ginouvès A, Volmat V, Roux D, Pouysségur J. HIF prolyl-hydroxylase 2 is the key oxygen sensor setting low steady-state levels of HIF-1alpha in normoxia. EMBO J. 2003 Aug 15;22(16):4082-90.

46. Cockman ME, Masson N, Mole DR, Jaakkola P, Chang GW, Clifford SC, Maher ER, Pugh CW, Ratcliffe PJ, Maxwell PH. Hypoxia inducible factor-alpha binding and ubiquitylation by the von Hippel-Lindau tumor suppressor protein. J Biol Chem. 2000 Aug 18;275(33):25733-41.

47. Maxwell PH, Wiesener MS, Chang GW, Clifford SC, Vaux EC, Cockman ME, Wykoff CC, Pugh CW, Maher ER, Ratcliffe PJ. The tumour suppressor protein VHL targets hypoxia-inducible factors for oxygen-dependent proteolysis. Nature. 1999 May 20;399(6733):271-5.

48. Burroughs SK, Kaluz S, Wang D, Wang K, Van Meir EG, Wang B. Hypoxia inducible factor pathway inhibitors as anticancer therapeutics. Future Med Chem. 2013 Apr;5(5):553-72.

49. Lopaschuk GD, Spafford MA, Marsh DR. Glycolysis is predominant source of myocardial ATP production immediately after birth. Am J Physiol. 1991 Dec;261(6 Pt 2):H1698-705.

50. Lopaschuk GD, Ussher JR, Folmes CD, Jaswal JS, Stanley WC. Myocardial fatty acid metabolism in health and disease. Physiol Rev. 2010 Jan;90(1):207-58.

51. Sack MN, Rader TA, Park S, Bastin J, McCune SA, Kelly DP. Fatty acid oxidation enzyme gene expression is downregulated in the failing heart. Circulation. 1996 Dec 1;94(11):2837-42.

52. Razeghi P, Young ME, Alcorn JL, Moravec CS, Frazier OH, Taegtmeyer H. Metabolic gene expression in fetal and failing human heart. Circulation. 2001 Dec 11;104(24):2923-31.

53. el Alaoui-Talibi Z, Landormy S, Loireau A, Moravec J. Fatty acid oxidation and mechanical performance of volume-overloaded rat hearts. Am J Physiol. 1992 Apr;262(4 Pt 2):H1068-74.

54. Baloglu E, Nonnenmacher G, Seleninova A, Berg L, Velineni K, Ermis-Kaya E, Mairbäurl H. The role of hypoxia-induced modulation of alveolar epithelial Na+- transport in hypoxemia at high altitude. Pulm Circ. 2020 Oct 13;10(1 Suppl):50-58.

55. Shannon P, Markiel A, Ozier O, Baliga NS, Wang JT, Ramage D, Amin N, Schwikowski B, Ideker T. Cytoscape: a software environment for integrated models of biomolecular interaction networks. Genome Res. 2003 Nov;13(11):2498-504.

56. Gene: HIF-1a (ENSRNOG00000008292) - Summary - Rattus_norvegicus - Ensembl genome browser 107. [2022 Jul 31]. Available from: https://www.ensembl.org/Rattus_norvegicus/Gene/Summary?db=core;g=ENSRNOG00000008292;r=6:92624390-92669261;t=ENSRNOT00000049725

57. "Quantification of Genome-Editing." Quantification of Genome Editing, www.crispr.technology/resources/quantification.html. (30.07.2022)

58. Bashir S, Banday M, Qadri O, Bashir A, Hilal N, Nida-I-Fatima, Rader S, Fazili KM. The molecular mechanism and functional diversity of UPR signaling sensor IRE1. Life Sci. 2021 Jan 15;265:118740.

59. Shamovsky I, Nudler E. New insights into the mechanism of heat shock response activation. Cell Mol Life Sci. 2008 Mar;65(6):855-61.

60. Yang L, Guell M, Byrne S, Yang JL, De Los Angeles A, Mali P, Aach J, Kim-Kiselak C, Briggs AW, Rios X, Huang PY, Daley G, Church G. Optimization of scarless human stem cell genome editing. Nucleic Acids Res. 2013 Oct;41(19):9049-61.

61. Allen PD, Schmidt TA, Marsh JD, Kjeldsen K. Na,K-ATPase expression in normal and failing human left ventricle. Basic Res Cardiol. 1992;87 Suppl 1:87-94.

62. Shamraj OI, Grupp IL, Grupp G, Melvin D, Gradoux N, Kremers W, Lingrel JB, De Pover A. Characterisation of Na/K-ATPase, its isoforms, and the inotropic response to ouabain in isolated failing human hearts. Cardiovasc Res. 1993 Dec;27(12):2229-37.

63. Schwinger RH, Bundgaard H, Müller-Ehmsen J, Kjeldsen K. The Na, K-ATPase in the failing human heart. Cardiovasc Res. 2003 Mar 15;57(4):913-20.

64. Kanehisa M, Goto S. KEGG: kyoto encyclopedia of genes and genomes. Nucleic Acids Res. 2000 Jan 1;28(1):27-30.

65. Parakh S, Atkin JD. Novel roles for protein disulphide isomerase in disease states: a double edged sword? Front Cell Dev Biol. 2015 May 21;3:30.

66. Shi X, Wang J, Lei Y, Cong C, Tan D, Zhou X. Research progress on the PI3K/AKT signaling pathway in gynecological cancer (Review). Mol Med Rep. 2019 Jun;19(6):4529-4535.

67. Dafforn TR, Della M, Miller AD. The molecular interactions of heat shock protein 47 (Hsp47) and their implications for collagen biosynthesis. J Biol Chem. 2001 Dec 28;276(52):49310-9.

68. Oslowski CM, Urano F. Measuring ER stress and the unfolded protein response using mammalian tissue culture system. Methods Enzymol. 2011;490:71-92.

69. Brahimi-Horn C, Pouysségur J. When hypoxia signalling meets the ubiquitin-proteasomal pathway, new targets for cancer therapy. Crit Rev Oncol Hematol. 2005 Feb;53(2):115-23.

70. Wouters BG, Koritzinsky M. Hypoxia signalling through mTOR and the unfolded protein response in cancer. Nat Rev Cancer. 2008 Nov;8(11):851-64.

71. Omari S, Makareeva E, Gorrell L, Jarnik M, Lippincott-Schwartz J, Leikin S. Mechanisms of procollagen and HSP47 sorting during ER-to-Golgi trafficking. Matrix Biol. 2020 Nov;93:79-94.

72. Kryvenko V, Wessendorf M, Tello K, Herold S, Morty RE, Seeger W, Vadász I. Hypercapnia Induces Inositol-Requiring Enzyme 1α-Driven Endoplasmic Reticulum-associated Degradation of the Na,K-ATPase β-Subunit. Am J Respir Cell Mol Biol. 2021 Dec;65(6):615-629.

73. Hoter A, El-Sabban ME, Naim HY. The HSP90 Family: Structure, Regulation, Function, and Implications in Health and Disease. Int J Mol Sci. 2018 Aug 29;19(9):2560.

74. Roberts RJ, Agius C, Saliba C, Bossier P, Sung YY. Heat shock proteins (chaperones) in fish and shellfish and their potential role in relation to fish health: a review. J Fish Dis. 2010 Oct;33(10):789-801.

75. Riordan M, Sreedharan R, Wang S, Thulin G, Mann A, Stankewich M, Van Why S, Kashgarian M, Siegel NJ. HSP70 binding modulates detachment of Na-K-ATPase following energy deprivation in renal epithelial cells. Am J Physiol Renal Physiol. 2005 Jun;288(6):F1236-42.

76. Ruete MC, Carrizo LC, Vallés PG. Na+/K+ -ATPase stabilization by Hsp70 in the outer stripe of the outer medulla in rats during recovery from a low-protein diet. Cell Stress Chaperones. 2008 Summer;13(2):157-67.

77. Umam K, Chuang HJ, Chiu L, Yang WK, Wang YC, Wu WY, Lee TH. Potential osmoprotective roles of branchial heat shock proteins towards Na+, K+-ATPase in milkfish (Chanos chanos) exposed to hypotonic stress. Comp Biochem Physiol A Mol Integr Physiol. 2020 Oct;248:110749.

78. Coppi MV, Guidotti G. Ubiquitination of Na,K-ATPase alpha1 and alpha2 subunits. FEBS Lett. 1997 Apr 1;405(3):281-4.

79. Helenius IT, Dada LA, Sznajder JI. Role of ubiquitination in Na,K-ATPase regulation during lung injury. Proc Am Thorac Soc. 2010 Feb;7(1):65-70.

80. Li H, Yang Y, Hong W, Huang M, Wu M, Zhao X. Applications of genome editing technology in the targeted therapy of human diseases: mechanisms, advances and prospects. Signal Transduct Target Ther. 2020 Jan 3;5(1):1.

7.APPENDIX

APPENDIX A: Chemicals Used in This Project

Chemicals and Other Components	Supplier Company, Catalog Number
Alfa (α1) NKA antibody	Abcam, #ab7671
Absolute Ethanol	Sigma, #32221
Acrylamide Solution	AppliChem, #UN3426
Alexa Flour Plus 555 Goat Anti-Rabbit	Thermo Scientific
Anti-Mouse Antibody	GE Healthcare, #NXA931
Anti-Rabbit Antibody	Calbiochem, #DC03L
Beta Actin Antibody	Sigma, #A2258
Bovine Serum Albumin	Sigma, #A2153-10G
Dulbecco's Phosphate-Buffered Saline	Sigma, #D8537
Ethidium Bromide	Sigma #e1510-10
EZ-Link Sulfo_NHS-ss-Biotin	Thermo Scientific, #21331
Fetal Bovine Serum	Capricorn, #FBS-11B
Gelatin	Sigma, #G9391
Gene Ruler DNALadder Mix	Thermo Scientific,#LSG-SM0331
HEPES	Sigma, # H 0887
HIF-1α antibody	Cell signaling, #D2U3T
Mouse IgG antibody	Cell Signaling, #5415

MyTaq™ DNA Polymerase	BIOLINE, #BIO-21105
Phusion® High-Fidelity DNA Polymerase	NEB, #M0530L
Protein A Agarose beads	Praesto jetted A50, Purolite
Proteinase K	Macherey-Nagel,#740506
PureLink®HiPure Midiprep Plasmid DNA Purification Kit	Invitrogen, #K210005
Puromycin	Sigma, #P8833
Streptavidin Agarose Resins	Pierce, Thermo Scientific
T7 Endonuclease I	NEB, #M0302S

APPENDIX B: Equipment Used in This Project

Equipment Supplier	**Company,Catalog Number**
T100™ Thermal Cycler PCR Machine	BioRad, #1861096
1.5 mL Microcentrifuge Tube	Capp, #5101500
100 mm Tissue Culture dish	Corning, #430167
96-well Tissue Cuture Plate	TPP, #92096
Cryovial Tube	TPP, #89020
Bacterial Cell Culture Incubator	Forma Steri-Cycle CO_2;Thermo Scientific, #521030301
Centrifuge Machine	Thermo Scientific, #SL16R
ChemiDoc Imaging System	BioRad, #1708265
Confocal microscope	Carl Zeiss, LSM700
Florescent Microscope	ZEIS AXIO Vert.A1
Gel Electrophoresis Casts	Major Science, #1406200009; VWR Mini Gel II, #95043-688
Microcentrifuge Machine	Thermo Scientific, #MicroCL21R
Microwave Oven	Samsung, #MW71E
Shaker	Stuart
Spectrophotometer	Hitachi Spectrophotometer, #U- 1900
Tissue Culture Incubator	Biorender
Vortex	VWR

APPENDIX C: DNA Ladder

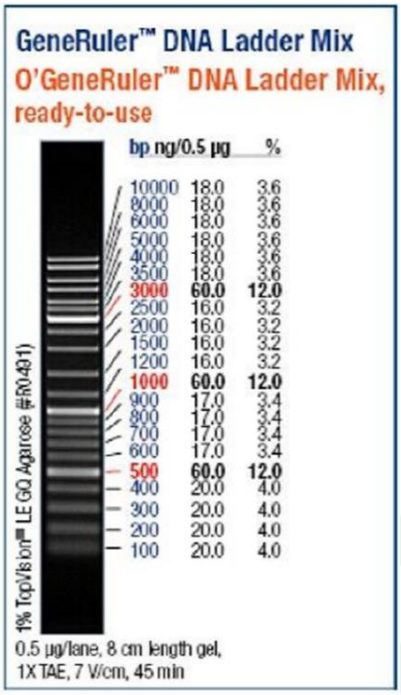

APPENDIX D: Protein Ladder

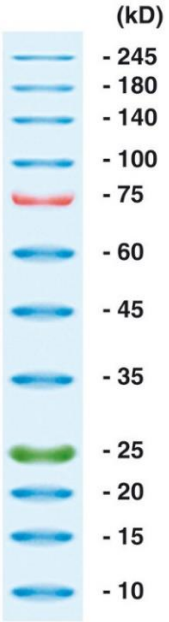

APPENDİX E : Plasmids that used for 3rd generation lentivirus production

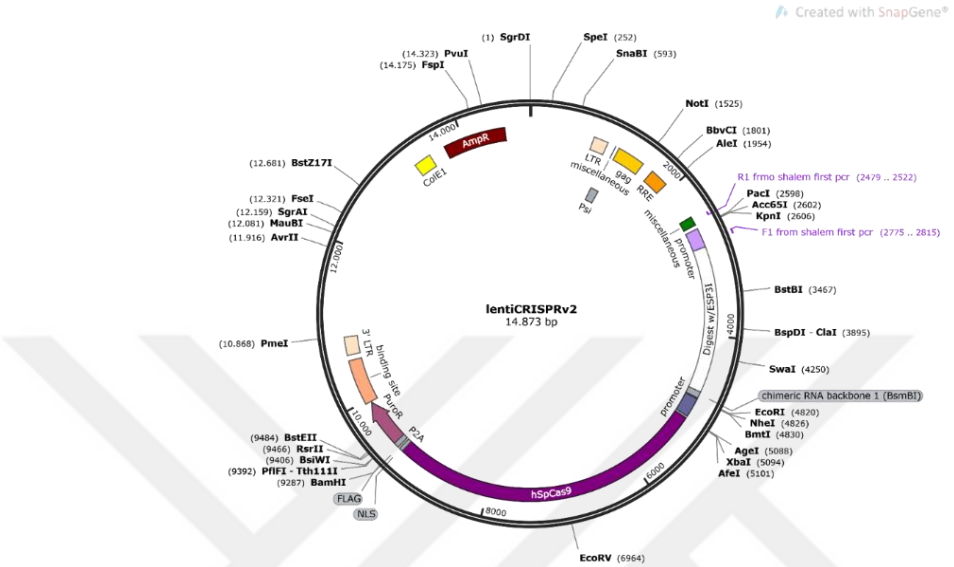

Map of the lentiCRISPRv2 plasmid. Mapped by Snap Gene Viewer 5.2.4**.** The plasmids have Cas9 endonuclease region (purple), puromycin resistance gene (pink) for transfected cells selection, ampicillin resistance gene (brown) for transformed bacterial cells selection and Esp3I cut region for cloning of designed guide RNA sequences.

A.

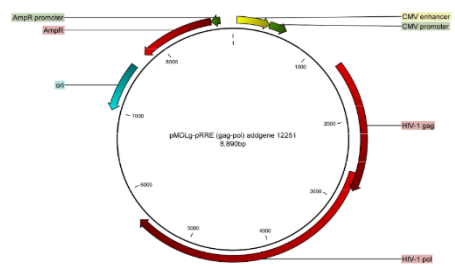

B.

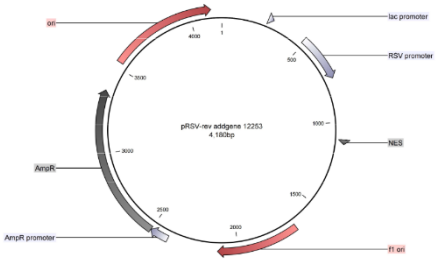

C.

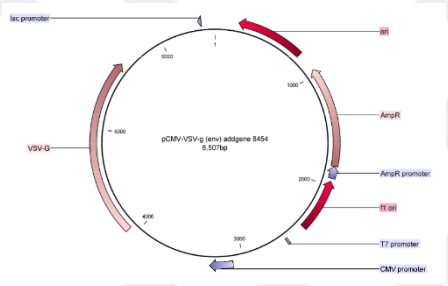

D.

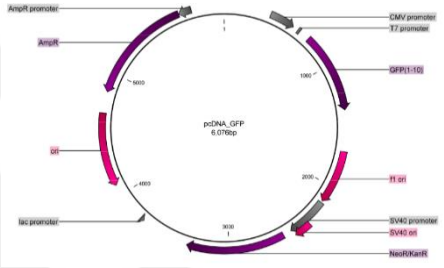

E.

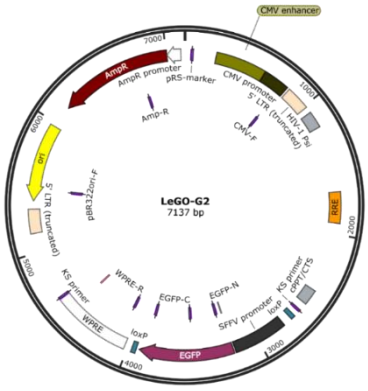

Maps of lentivirus production plasmids A. pMDLg/pRRE (Addgene #12251) **B.** pRSV-rev (Addgene #12253**) C.** pCMV-VSV-g (Addgene #8454) **D.** pcDNA GFP **E.** Lego G2

8. CURRICULUM VITAE